Ancestral mitochondrial apparatus derived from the bacterial type II secretion system

Lenka Horváthová[1*], Vojtěch Žárský[1*], Tomáš Pánek[2*$], Romain Derelle[3], Jan Pyrih[4], Alžběta Motyčková[1], Veronika Klápšťová[1], Martina Vinopalová[1], Lenka Marková[1], Luboš Voleman[1], Vladimír Klimeš[2], Markéta Petrů[1], Zuzana Vaitová[1], Ivan Čepička[5], Klára Hryzáková[6], Karel Harant[7], Michael W. Gray[8], Mohamed Chami[9], Ingrid Guilvout[10], Olivera Francetic[10], B. Franz Lang[11], Čestmír Vlček[12], Anastasios D. Tsaousis[4], Marek Eliáš[2#], Pavel Doležal[1#]

[1]Department of Parasitology, Faculty of Science, Charles University, BIOCEV, Průmyslová 595, Vestec, 252 42, Czech Republic
[2]Department of Biology and Ecology, Faculty of Science, University of Ostrava, Chittussiho 10, 710 00 Ostrava, Czech Republic
[3]School of Biosciences, University of Birmingham, Edgbaston, B15 2TT, UK
[4]Laboratory of Molecular & Evolutionary Parasitology, RAPID group, School of Biosciences, University of Kent, Canterbury, CT2 7NZ, UK
[5]Department of Zoology, Faculty of Science, Charles University, Viničná 7, Prague 2, 128 44, Czech Republic
[6]Department of Genetics and Microbiology, Faculty of Science, Charles University, Viničná 7, Prague 2, 128 44, Czech Republic[7]Proteomic core facility, Faculty of Science, Charles University, BIOCEV, Průmyslová 595, Vestec, 252 42, Czech Republic
[8]Department of Biochemistry and Molecular Biology and Centre for Comparative Genomics and Evolutionary Bioinformatics, Dalhousie University, Halifax, NS B3H 4R2, Canada
[9]Center for Cellular Imaging and NanoAnalytics, University of Basel, Mattenstrasse 26, CH-4058 Basel, Switzerland
[10]Institut Pasteur, Biochemistry of Macromolecular Interactions Unit, Department of Structural Biology and Chemistry, CNRS UMR3528, 75015 Paris, France
[11]Robert Cedergren Centre for Bioinformatics and Genomics, Département de Biochimie, Université de Montréal, Montreal, QC, Canada H3T 1J4
[12]Institute of Molecular Genetics, Czech Academy of Sciences, 142 20 Prague 4, Czech Republic
[$]Current address: Department of Zoology, Faculty of Science, Charles University, Viničná 7, Prague 2, 128 44, Czech Republic

*these authors equally contributed to the study
#corresponding authors: Marek Eliáš (marek.elias@osu.cz), Pavel Doležal (pavel.dolezal@natur.cuni.cz)

Abstract

The type 2 secretion system (T2SS) is present in some Gram-negative eubacteria and used to secrete proteins across the outer membrane. Here we report that certain representative heteroloboseans, jakobids, malawimonads and hemimastigotes unexpectedly possess homologues of core T2SS components. We show that at least some of them are present in mitochondria, and their behaviour in biochemical assays is consistent with the formation of a mitochondrial T2SS-derived protein secretion system (miT2SS). We additionally identified 23 protein families co-occurring with miT2SS in eukaryotes. Seven of these proteins could be directly linked to the core miT2SS by functional data and/or sequence features, whereas others may represent different parts of a broader functional pathway, possibly also involving the peroxisome. Its distribution in eukaryotes and phylogenetic evidence together indicate that the miT2SS-centred pathway is an ancestral eukaryotic trait. Our findings thus have direct implications for the functional properties of the early mitochondrion.

Introduction

Mitochondria of all eukaryotes arose from the same Alphaproteobacteria-related endosymbiotic bacterium[1,2]. New functions have been incorporated into the bacterial blueprint during mitochondrial evolution, while many ancestral traits have been lost. Importantly, in some cases, these losses occurred independently in different lineages of eukaryotes, resulting in a patchy distribution of the respective ancestral mitochondrial traits in extant eukaryotes. Examples are the ancestral mitochondrial division apparatus (including homologues of bacterial Min proteins), the aerobic-type rubrerythrin system, or the tmRNA-SmpB complex, each retained in different subsets of distantly related protist lineages[3–5]. It is likely that additional pieces of the ancestral bacterial cell physiology will be discovered in mitochondria of poorly studied eukaryotes.

An apparent significant difference between the mitochondrion and bacteria (including those living as endosymbionts of eukaryotes) lies in the directionality of protein transport across their envelope. All bacteria export specific proteins from the cell via the plasma membrane using the Sec or Tat machineries[6], and many diderm (Gram-negative) bacteria exhibit specialized systems mediating further protein translocation across the outer membrane (OM)[7]. In contrast, the mitochondrion depends on a newly evolved protein import system spanning both envelope membranes and enabling import of proteins encoded by the nuclear genome[8]. The capacity of mitochondria to secrete proteins seems to be limited. Mitochondrial homologues of Tat translocase subunits occur in some eukaryotic taxa, but their role in protein secretion has not been established[9,10]. A mitochondrial homologue of the SecY protein (a Sec translocase subunit) has been described only in jakobids[11,12] and its function remains elusive[13]. No dedicated machinery for protein export from the mitochondrion across the outer mitochondrial membrane has been described.

One of the best characterized bacterial protein translocation machineries is the so-called type 2 secretion system (T2SS)[14,15]. The T2SS belongs to a large bacterial superfamily of type 4 pili (T4P)-related molecular machines, most of which secrete long extracellular filaments (pili) for motility, adhesion, or DNA uptake[16–18]. The T2SS constitutes a specialized secretion apparatus, whose filament (pseudopilus) remains in the

periplasm[14,15]. It is composed of 12-15 conserved components, commonly referred to as general secretion pathway (Gsp) proteins, which assemble into four main subcomplexes (Fig. 1A). The OM pore is formed by an oligomer of 15-16 molecules of the GspD protein[19,20]. The subcomplex in the inner membrane (IM) is called the assembly platform and consists of the central polytopic membrane protein GspF surrounded by single-pass membrane proteins GspC, GspL, and GspM[21]. GspC links the assembly platform to the OM pore by interacting with the periplasmic N-terminal domain of GspD[22,23]. The third subcomplex, called the pseudopilus, is a helical filament formed mainly of GspG subunits, with minor pseudopilins (GspH, GspI, GspJ and GspK) assembled at its tip[24]. Pseudopilus assembly from its inner membrane base is believed to push the periplasmic T2SS substrate through the OM pore. The energy for pseudopilus assembly is provided by the fourth subcomplex, the hexameric ATPase GspE, interacting with the assembly platform from the cytoplasmic side[25,26]. Substrates for T2SS-mediated secretion are first transported by the Tat (as folded proteins) or the Sec (in an unfolded form) system across the IM into the periplasm, where they undergo maturation and/or folding. The folded substrates are finally loaded onto the pseudopilus for the release outside the cell via the OM pore. The known T2SS substrates differ among taxa and share no common sequence or structural features. Proteins transported by the T2SS in different species include catabolic enzymes (such as lipases, proteases or phosphatases) and, in the case of bacterial pathogens, toxins[14]. A recent survey of bacterial genomes showed that the T2SS is mainly present in Proteobacteria[18]. Crucially, neither the T2SS nor other systems of the T4P superfamily have been reported from eukaryotes[7,14,18].

Here we show that certain distantly related eukaryotes unexpectedly contain homologues of key T2SS subunits representing all four functional T2SS subcomplexes. We provide evidence for mitochondrial localization of some of these eukaryotic Gsp protein homologues and describe experimental results supporting the idea that they constitute a system similar to the bacterial T2SS. Furthermore, we point to the existence of 23 proteins with a perfect taxonomic co-occurrence with the eukaryotic Gsp homologues. Some of these co-occurring proteins seem to be additional components of the mitochondrial T2SS-related machinery, whereas others are candidates for components of a broader functional pathway linking the mitochondrion with other parts of the cell. Given its phylogenetic distribution, we propose that the newly discovered pathway was ancestrally present in eukaryotes. Its further characterization may provide fundamental new insights into the evolutionary conversion of the protomitochondrion into the mitochondrial organelle.

Results

Certain protist lineages code for a conserved set of homologues of T2SS core components

While searching the genome of the heterolobosean *Naegleria gruberi* for proteins of bacterial origin with a possible mitochondrial role, we surprisingly discovered homologues of four core subunits of the bacterial T2SS, specifically GspD, GspE, GspF, and GspG (Fig. 1A; Supplementary Table 1). Using genomic and transcriptomic data from public repositories and our on-going sequencing projects for several protist species of key evolutionary interest (see Methods), we mapped the distribution of these four components in eukaryotes. All four genes were found in the following characteristic set

139 of taxa (Fig. 1B, Supplementary Table 1): three additional heteroloboseans (*Naegleria*
140 *fowleri*, *Neovahlkampfia damariscottae*, *Pharyngomonas kirbyi*), two jakobids (*R.*
141 *americana* and *Andalucia godoyi*), and two malawimonads (*Malawimonas jakobiformis*
142 and *Gefionella okellyi*). In addition, single-cell transcriptomes from two species of
143 Hemimastigophora (hemimastigotes[27]) revealed the presence of homologues of GspD and
144 GspG (*Hemimastix kukwesjijk*) and GspG only (*Spironema* cf. *mulitciliatum*), possibly
145 reflecting incompleteness of the data. Finally, three separate representatives of the
146 heterolobosean genus *Percolomonas* (Supplementary Fig. 1) each exhibited a homologue
147 of GspD, but not of the remaining Gsp proteins, in the available transcriptomic data. In
148 contrast, all four genes were missing in sequence data from all other eukaryotes
149 investigated, including the genome and transcriptome of another malawimonad
150 ("Malawimonas californiana") and deeply-sequenced transcriptomes of a third jakobid
151 (*Stygiella incarcerata*) and four additional heteroloboseans (*Creneis carolina*,
152 *Dactylomonas venusta*, *Harpagon schusteri*, and the undescribed strain Heterolobosea sp.
153 BB2).
154 Probing *N. gruberi* nuclei with fluorescence *in situ* hybridization ruled out an
155 unidentified bacterial endosymbiont as the source of the *Gsp* genes (Supplementary Fig.
156 2). Moreover, the eukaryotic *Gsp* genes usually have introns and constitute robustly
157 supported monophyletic groups well separated from bacterial homologues (Fig. 2;
158 Supplementary Fig. 3), ruling out bacterial contamination in all cases. In an attempt to
159 illuminate the origin of the eukaryotic Gsp proteins we carried out systematic
160 phylogenetic analyses based on progressively expanded datasets of prokaryotic
161 homologues and for each tree inferred the taxonomic identity of the bacterial ancestor of
162 the eukaryotic branch (see Methods for details on the procedure). The results,
163 summarized in Supplementary Fig. 3, showed that the inference is highly unstable
164 depending on the dataset analysed, and no specific bacterial group can be identified as an
165 obvious donor of the eukaryotic Gsp genes. This result probably stems from a
166 combination of factors, including the long branches separating the eukaryotic and
167 bacterial Gsp sequences, the length of Gsp proteins restricting the amount of the
168 phylogenetic signal retained, and perhaps also rampant horizontal gene transfer (HGT) of
169 the T2SS system genes between bacterial taxa. The eukaryotic Gsp genes are in fact so
170 divergent that some of them could not be unambiguously classified as specific
171 homologues of T2SS components (rather than the related machineries of the T4P
172 superfamily) when analysed using models developed for the bacterial genomes[18]
173 (Supplementary Fig. 3).
174 Heteroloboseans, jakobids and malawimonads have been classified in the
175 supergroup Excavata[28]. However, recent phylogenomic analyses indicate that excavates
176 are non-monophyletic and even suggest that malawimonads are separated from
177 heteroloboseans and jakobids by the root of the eukaryote phylogeny[29–32]. Together with
178 the presence of at least some Gsp proteins in hemimastigotes, which constitute an
179 independent eukaryotic supergroup[27], it is likely that the T2SS-related proteins were
180 present in the last eukaryotic common ancestor (LECA) but lost in most eukaryote
181 lineages (Fig. 1B). Heteroloboseans and malawimonads have two GspG paralogues, but
182 the phylogenetic analyses did not resolve whether this is due to multiple independent
183 GspG gene duplications or one ancestral eukaryotic duplication followed by loss of one
184 of the paralogues in jakobids (Fig. 2; Supplementary Fig. 3D; Supplementary Table 1).

The eukaryotic Gsp proteins localize to the mitochondrion

We hypothesized that the eukaryotic homologues of the four Gsp proteins are parts of a functional T2SS-related system localized to the mitochondrion. This notion was supported by the presence of predicted N-terminal mitochondrial targeting sequences (MTSs) in some of the eukaryotic Gsp proteins (Supplementary Table 1). The prediction algorithms identified putative N-terminal MTSs for proteins from jakobids and malawimonads but failed to recognize them in the orthologues from heteroloboseans, which, however, carry the longest N-terminal extensions (Supplementary Fig. 4).

In order to test if Gsp proteins carry functional mitochondrial targeting information, we expressed *GspD*, *GspE* and *GspG1* genes from *N. gruberi* (*Ng*) and *G. okellyi* (*Go*) in *Saccharomyces cerevisiae*; no expression of *GspF* was achieved. All proteins were specifically localised in mitochondria, as confirmed by their co-localisation with Mitotracker red CMX Ros (Fig. 3A). Additionally, we attempted to express these genes in *Trypanosoma brucei*, which represents the evolutionarily closest experimental model to the eukaryotes carrying the *Gsp* genes. Of all the proteins tested, only *Go*GspD and *Go*GspG2 were detected (Fig. 3B), in addition to a weak signal for *Ng*GspG1 (Supplementary Fig. 5A). While both GspG proteins could be found specifically in the mitochondrion of *T. brucei*, *Go*GspD was found in a different membrane compartment, perhaps due to mistargeting. Finally, we tested if the atypically long N-terminal extension of *Ng*GspG1 targets the protein to the *T. brucei* mitochondrion. Indeed, the 160 N-terminal amino acid residues of *Ng*GspG1 were able to deliver the marker (mNeonGreen) into the organelle (Supplementary Fig. 5B). As a complementary approach, we raised specific polyclonal antibodies against *Ng*GspG1 and probed *N. gruberi* cellular fractions (Fig. 3C; Supplementary Fig. 6). *Ng*GspG1 and *Ng*GspEN2A co-fractionated with the mitochondrial markers including alternative oxidase (AOX) and TatC[9], but not with the cytosolic protein hemerythrin[33]. Immunofluorescence microscopy of *N. gruberi* with the anti-*Ng*GspG1 antibody provided further evidence that *Ng*GspG1 is targeted to mitochondria (Fig. 3D, Supplementary Fig. 7).

In order to further confirm the mitochondrial localization of the Gsp proteins in *N. gruberi*, we analysed the mitochondrial proteome of this organism by partial purification of the organelle and identification of resident proteins by mass spectrometry. A mitochondria-enriched fraction was obtained from a cellular lysate by several steps of differential centrifugation and OptiPrep gradient centrifugation. Three sub-fractions of different densities were collected (Supplementary Fig. 8A), with the densest one being most enriched in mitochondria. The fractions were subjected to proteomic analysis. The relative amount of each protein in the gradient was determined by label-free quantification and the proteins were grouped by a multicomponent analysis (for details see Methods) according to their distributions across the gradient (Fig. 3E). A set of marker proteins (homologues of well-characterized typical mitochondrial proteins from other species) was used to identify a cluster of mitochondrial proteins. Due to the partial co-purification of peroxisomes with mitochondria, a peroxisome-specific cluster was defined analogously. As a result, 946 putative mitochondrial and 78 putative peroxisomal proteins were identified among the total of 4,198 proteins detected in all three sub-fractions combined. Encouragingly, the putative mitochondrial proteome of *N. gruberi* is dominated by proteins expected to be mitochondrial or whose mitochondrial localization

is not unlikely (Supplementary Fig. 8B, Supplementary Table 2A). On the other hand, the putative peroxisomal proteome seems to be contaminated by mitochondrial proteins (owing to the presence of several mitochondrial ribosomal proteins; Supplementary Table 2B). Importantly, all five Gsp proteins (including both GspG paralogues) were identified in the putative mitochondrial but not peroxisomal proteome of *N. gruberi*.

The properties of the eukaryotic Gsp proteins support the existence of a mitochondrial T2SS-related machinery

The foregoing experiments support the idea that all four eukaryotic Gsp homologues localize to and function in the mitochondrion. However, direct *in vivo* demonstration of the existence of a functional mitochondrial T2SS-related machinery is currently not feasible, because none of the Gsp homologue-carrying eukaryotes represents a tractable genetic system. We thus used *in vitro* approaches and heterologous expression systems to test the key properties of the eukaryotic Gsp proteins.

Crucial for the T2SS function is the formation of the OM pore, which is a β-barrel formed by the oligomerization of the C-domain of the GspD protein[34]. The actual assembly of the bacterial pore requires GspD targeting to the outer membrane through interaction of its very C-terminal domain (S-domain) with the outer membrane lipoprotein GspS[35]. GspD forms a pre-pore multimer, whose OM membrane insertion is independent on the β-barrel assembly machinery (BAM) complex[36,37]. In addition, the bacterial GspD carries four short N-terminal domains exposed to the periplasm, called N0 to N3, of which N1 to N3 share a similar fold[38] (Fig. 4A). While the N3 domain is required for the pore assembly[39], N0 interacts with GspC of the assembly platform[22,40]. Sequence analysis of the mitochondrial GspD homologue revealed that it corresponds to a C-terminal part of the bacterial GspD C-domain, whereas the N-terminal domains N0 to N3, the N-terminal part of the C-domain, and the S-domain are missing (Fig. 4A; Supplementary Fig. 4A).

According to our hypothesis, the mitochondrial GspD should be present in the outer mitochondrial membrane. In order to test this localization, *N. gruberi* GspD (*Ng*GspD) was *in vitro* imported into yeast mitochondria. The import reaction was also performed with the widely used synthetic substrate Su9-DHFR destined to mitochondrial matrix, which is composed of 69 amino acid residues of F_o-ATPase subunit 9 from *Neurospora crassa* fused to the mouse DHFR[41]. Both proteins accumulated in the mitochondria in a time-dependent manner, but only the import of Su9-DHFR could be inhibited by the addition of ionophores, which dissipate membrane potential ($\Delta\Psi$) (Fig. 4B). This result showed that the import of GspD is independent of $\Delta\Psi$, which is a typical feature of mitochondrial outer membrane proteins. The key question was if the mitochondrial GspD homologue has retained the ability to assemble into an oligomeric pore-forming complex. This possibility was supported by homology modelling of GspD from *G. okellyi* (*Go*GspD) using *Vibrio cholerae* GspD[42] as a template, which indicated that the protein has the same predicted fold as the typical secretin C-domain. Remarkably, the two transmembrane β-strands of *Go*GspD are separated by the highly conserved amphipathic helical loop (AHL) (Fig. 4C) essential for secretin membrane insertion, suggesting its capability to form a pentadecameric pore complex. Indeed, radioactively labelled *Go*GspD assembled into a high-molecular-weight complex of around 200 kDa in an *in vitro* bacterial translation system in the presence of lecithin liposomes (Fig. 4D).

277 The complex was resistant to 2M urea treatment, which would remove nonspecific
278 protein aggregates, and was still pelleted with the liposomes, suggesting that it was
279 inserted into the liposomes. These results showed that the mitochondrial GspD, despite
280 being significantly truncated when compared to its bacterial homologues, has retained the
281 major characteristics of bacterial secretins[43], including the capacity to form oligomers and
282 insert into membranes.
283 To test if the mitochondrial GspD forms *bona fide* pores in the membrane, we
284 aimed to produce His-tagged *Ng*GspD in *E. coli* and purify the membrane complexes for
285 the electrophysiology analysis. Inducing the production of this protein in the bacterial
286 cytoplasm was highly toxic (Fig. 5A). A similar phenomenon has been reported for
287 bacterial secretins, which form pores in the inner bacterial membrane[43]. While this
288 hampered protein production and purification, directing the GspD export to the periplasm
289 by fusing it to the N-terminal signal peptide of *E. coli* DsbA protein alleviated the
290 toxicity upon autoinduction. The His-*Ng*GspD variant was affinity-purified on a Ni-
291 column followed by size exclusion chromatography, during which two peaks of about
292 230 kDa and 125 kDa could be observed (Fig. 5B). The pore-forming activity of His-
293 *Ng*GspD purified from both protein peaks was demonstrated by conductivity
294 measurements in black lipid membranes composed of an *E. coli* polar lipid extract. The
295 channel recordings illustrated a very high stability of the inserted membrane pores (Fig.
296 5C). The amplitude histograms (Fig. 5D) suggested that the mitochondrial GspD can
297 form variable arrangements resulting in stable membrane pores of different sizes.
298 The secretion mechanism of the T2SS relies on the assembly of pseudopilus made
299 up of GspG subunits[44]. Comparison of the mitochondrial GspG with bacterial
300 homologues revealed important similarities as well as differences. These proteins share a
301 complete pseudopilin domain preceded by a transmembrane domain, but the
302 mitochondrial proteins are substantially longer due to extensions at both N- and C-termini
303 (Fig. 6A). The N-terminal extension likely serves as a MTS, but the origin and function
304 of the C-terminal extension (amounting to ~100 amino acid residues) is unclear, as it is
305 well conserved among the mitochondrial GspG but lacks discernible homologues even
306 when analysed by highly sensitive homology-detection methods (HMM-HMM
307 comparisons with HHpred[45] and protein modelling using the Phyre2 server[46]). Structural
308 modelling of the pseudopilin domain into the recently obtained cryo-EM reconstruction
309 of the PulG (=GspG) complex from *Klebsiella oxytoca*[47] revealed the presence of key
310 structural features in the mitochondrial GspG from *G. okellyi* (*Go*GspG1), supporting
311 possible formation of a pseudopilus (Fig. 6B).
312 To test this directly, we purified a recombinant pseudopilin domain of *Ng*GspG1
313 under native conditions, which showed a uniform size of 25 kDa corresponding to the
314 monomer (Fig. 7A). Possible protein-protein interaction of the purified pseudopilin
315 domain was tested by thermophoresis of an NT-647-labelled protein. The measurements
316 revealed specific self-interaction and plotting of the change in thermophoresis yielded a
317 K_d of 216 (±15.1) nM (Fig. 7B). Additionally, the interaction properties of GspG were
318 followed by the bacterial two-hybrid assay (BACTH). When produced in bacteria, the
319 mitochondrial *Go*GspG1 showed specific oligomerisation, typical of bacterial major
320 pseudopilins[48], supporting its *in vivo* propensity to form a pseudopilus (Fig. 7C). An
321 analogous BACTH assay of *N. gruberi* Gsp proteins also showed GspG1 self-interaction
322 (data not shown). In addition, *Go*GspG1 showed positive interaction with *Go*GspF,

consistent with the analogous interaction of bacterial GspG with the IM-embedded GspF[48]. Moreover, the mitochondrial *Go*GspF and *Go*GspE each formed dimers in the BACTH assay (Fig. 7C). These interactions are consistent with the hypothesized role of both proteins as mitochondrial T2SS components, as GspF forms dimers within the IM complex and GspE assembles into an active hexameric ATPase in the bacterial T2SS system. Indeed, bacterial GspG and GspF also interact in the BACTH assay[48]. Tests of all other possible interactions of *G. okellyi* Gsp proteins were negative.

The *in silico* analyses and experiments described above are consistent with the hypothesized existence of a functional mitochondrial secretion machinery derived from the bacterial T2SS. However, the mitochondrial subunits identified would assemble only a minimalist version of the secretion system, reduced to the functional core of the four subcomplexes of the bacterial T2SS, i.e. the luminal ATPase (GspE), the IM pseudopilus assembly platform (GspF), the intermembrane space pseudopilus (GspG), and the OM pore (truncated GspD). Despite using sensitive HMM-based searches, we did not detect homologues of other conserved T2SS subunits in any of the eukaryotes possessing GspD to GspG proteins. One of the missing subunits is GspC, which connects the assembly platform with the N0 domain of GspD pore[22,23]. Thus, the absence of GspC in eukaryotes correlates with the lack of the N0 domain in the eukaryotic GspD. Analogously, the absence of the C-terminal S-domain in the mitochondrial GspD (Fig. 4A), known to be missing also from some bacterial GspD proteins, rationalizes the lack of a eukaryotic homologue of the bacterial OM component GspS that binds to GspD via the S-domain during the pore assembly[35]. The apparent lack of a eukaryotic homologue of GspL, which interacts via its cytosolic domain with the N1E domain of the bacterial GspE [49], may similarly be explained by the fact that the eukaryotic GspE protein seems to be homologous only to the C-terminal (CTE) domain of its bacterial counterpart and lacks an equivalent of the N1E domain (Supplementary Fig. 4E). The mitochondrial system also apparently lacks a homologue of GspO, a bifunctional enzyme that is essential for GspG maturation. Despite this absence, eukaryotic GspG homologues have conserved all the characteristic sequence features required for GspG maturation (the polar anchor and the trans-membrane domain with a conserved glutamate residue at position +5 relative to the processing site) (Fig. 6A, Supplementary Fig. 4J). Notably, all the *Ng*GspG1 and *Ng*GspG2-derived peptides detected in our proteomic analysis come from the region of the protein downstream of the conserved processing site (Fig. 6C), suggesting that analogous maturation of the pseudopilin also occurs in mitochondria.

New putative components of the mitochondrial T2SS-based functional pathway identified by phylogenetic profiling

Since none of the eukaryotes with the Gsp homologues is currently amenable to functional studies, we tried to further illuminate the role of the mitochondrial T2SS system using a comparative genomic approach. Specifically, we reasoned that possible additional components of the machinery, as well as its actual substrate(s), might show the same phylogenetic distribution as the originally identified four subunits. Using a combination of an automated identification of candidate protein families and subsequent manual scrutiny by exhaustive searches of available eukaryote sequence data (for details of the procedure see Methods), we identified 23 proteins (more precisely, groups of orthologues) that proved to exhibit the same phylogenetic distribution in eukaryotes as

369 the four core T2SS components. Specifically, all 23 proteins were represented in each of
370 the heterolobosean, jakobid, and malawimonad species possessing all four core Gsp
371 proteins, whereas only 17 proteins were identified in the incomplete transcriptomic data
372 of hemimastigotes and seven of them were found in the transcriptomic data from the
373 *Percolomonas* lineage that possesses only GspD (Fig. 1B; Supplementary Table 1).
374 Except for two presumably Gsp-positive jakobids represented by incomplete EST surveys
375 and a case of a likely contamination (Supplementary Table 3), no orthologues of any of
376 these proteins were found in any other eukaryote (including the Gsp-lacking members of
377 heteroloboseans, jakobids and malawimonads). The sequences of these 23 proteins were
378 analysed by various *in silico* approaches, including HHpred and Phyre2 to assess their
379 possible function (Fig. 8A).
380 These analyses revealed that seven of the families have a direct link to the T2SS
381 suggested by discerned homology to known T2SS components. One of them represents
382 an additional, more divergent homologue of the C-terminal part of the bacterial GspD.
383 Hence, the protein has been marked as GspDL (GspD-like). Three other families, referred
384 to as GspDN1 to GspDN3, proved to be homologous to the Secretin_N domain (Pfam
385 family PF03958), present in the bacterial GspD protein as domains N1, N2 and N3 (Fig.
386 4A). The N1-N3 array protrudes into the periplasm, where it oligomerizes to form three
387 stacked rings[20]. As mentioned above, the initially identified eukaryotic GspD homologues
388 lack the N-terminal region, suggesting that the gene was split into multiple parts in
389 eukaryotes. While GspDN1 corresponds to a full single N-domain, GspDN2 and GspDN3
390 relate only to its C-terminal and N-terminal halves, respectively (Fig. 4A; Supplementary
391 Fig. 4B-D). Unfortunately, high sequence divergence makes it impossible to identify
392 potential specific correspondence between the N1 to N3 domains of the bacterial GspD
393 and the eukaryotic GspDN1 to GspDN3 proteins. Importantly, a Y2H assay indicated that
394 the two separate polypeptides GspD and GspDN1 of *N. gruberi* may interact *in vivo* (Fig.
395 4E), perhaps forming a larger mitochondrial complex. In addition, we identified most of
396 the newly discovered GspD-related proteins (GspDL/N) in the *N. gruberi* mitochondrial
397 proteome (the exception being GspDN1, which was not detected in a sufficient number of
398 replicates to be included in the downstream analysis; Supplementary Table 2A).
399 The final three proteins linked to the T2SS based on their sequence features seem
400 to be evolutionarily derived from GspE. One, denoted GspEL (GspE-like) represents a
401 divergent homologue of the C1E (i.e. nucleotide-binding) domain of GspE, although with
402 some of the characteristic motifs (Walker A, Asp box, Walker B) abrogated
403 (Supplementary Fig. 4F), indicating the loss of the ATPase function. The other two
404 proteins, which we denote GspEN2A and GspEN2B, are suggested by HHpred to be
405 related to just the N2E domain of the bacterial GspE (Supplementary Fig.4G and 4H).
406 GspEN2A and GspEN2B were identified among *N. gruberi* mitochondrial proteins in the
407 proteomic analysis, whereas GspEL was found in the cluster of putative peroxisomal
408 proteins. Importantly, a polyclonal antibody raised against *Ng*GspEN2A confirmed the
409 mitochondrial localization of the protein (Fig. 3C, D; Supplementary Fig. 6, 7).
410 The remaining sixteen proteins co-occurring with the core eukaryotic T2SS
411 subunits, hereafter referred to as Gcp (Gsp-co-occurring proteins), were divided into three
412 categories. The first comprises four proteins that constitute novel paralogues within
413 broader common eukaryotic (super)families. Three of them (Gcp1 to Gcp3) belong to the
414 WD40 superfamily and seem to be most closely related to the peroxisomal protein import

415 co-receptor Pex7 (Supplementary Fig. 9). None of these proteins has any putative N-
416 terminal targeting sequence, but interestingly, the peroxisomal targeting signal 1 (PTS1)
417 could be predicted on most Gcp1 and some Gcp2 proteins (Supplementary Table 1).
418 However, these predictions are not fully consistent with the results of our proteomic
419 analysis: *Ng*Gcp1 was found among the mitochondrial proteins and *Ng*Gcp2 in the cluster
420 of putative peroxisomal proteins (Supplementary Table 2), but PTS1 is predicted to be
421 present in the *Ng*Gcp1 protein (Supplementary Table 1). The fourth Gcp protein (Gcp4)
422 is a novel paralogue of the ubiquitin-like superfamily, distinctly different from the
423 previously characterized members including ubiquitin, SUMO, NEDD8 and others
424 (Supplementary Fig. 10).
425 The second Gcp category comprises eleven proteins (Gcp5 to Gcp15) well
426 conserved at the sequence level among the Gsp-containing eukaryotes, yet lacking any
427 discernible homologues in other eukaryotes or in prokaryotes. Two of these proteins
428 (Gcp8, Gcp15) were not identified in the proteomic analysis of *N. gruberi*
429 (Supplementary Tables 1 and 2). Of those identified, several (Gcp5, Gcp6, Gcp13) were
430 found among the mitochondrial proteins, whereas some others (Gcp9, Gcp10, Gcp11)
431 clustered with peroxisomal markers. Specific localization of the three remaining proteins
432 (Gcp7, Gcp12, and Gcp14) could not be determined due to their presence at the
433 boundaries of the mitochondrial or peroxisomal clusters. No homology to other proteins
434 or domains could be discerned for the Gsp5 to Gsp15 proteins even when sensitive
435 homology-detection algorithms were employed. However, four of them are predicted as
436 single-pass membrane proteins, with the transmembrane segment in the N- (Gcp7,
437 Gcp11, Gcp15) or C-terminal (Gcp5) regions (Fig. 8A; Supplementary Fig. 11).
438 Interestingly, Gcp6 and Gcp12 proteins contain multiple absolutely conserved cysteine or
439 histidine residues (Fig. 8A, B; Supplementary Fig. 12). We were not able to determine
440 their localization in *N. gruberi* by microscopy, but we tested the localization of *Go*Gcp12
441 upon expression in *T. brucei*, where it co-localized with the mitochondrial tubules (Fig.
442 8C).
443 Gcp16 constitutes a category of its own, as it typifies a novel protein family
444 present also in bacteria of the PVC superphylum (Supplementary Fig. 13). Phylogenetic
445 analysis confirmed that the eukaryotic members of the family are of the same origin
446 (Supplementary Fig. 14). Gcp16 proteins are predicted to harbour two transmembrane
447 domains (Supplementary Fig. 13). Furthermore, HHpred searches suggested possible
448 homology of a region of the Gcp16 protein (upstream of the transmembrane domains) to
449 various metallopeptidases, although with inconclusive statistical support. However,
450 inspection of the HHpred alignments revealed that Gcp16 shares with these hits an
451 absolutely conserved motif HEXXH (Supplementary Fig. 13), which is the catalytic,
452 metal-binding motif of the zincin tribe of metallopeptidases[50]. Interestingly, close to the
453 HEXXH motif, Gcp16 possesses an absolutely conserved EXXA motif, which is
454 diagnostic of a zincin subgroup called gluzincins[50], further supporting the notion that
455 Gcp16 may function as a membrane-embedded peptidase. Most eukaryotic Gcp16
456 proteins exhibit an N-terminal extension compared to the bacterial homologues
457 (Supplementary Fig. 13), but only some of these extensions are recognized as putative
458 MTSs and the *N. gruberi* Gcp16 was not identified either in putative mitochondrial or
459 peroxisomal proteome.
460

Discussion

Our analyses revealed that a subset of species belonging to four eukaryotic lineages share a set of at least 27 proteins (or families of orthologues) absent from other eukaryotes for which genomic or transcriptomic data are currently available (Fig. 1B). At least eleven of these proteins (the Gsp proteins) are evolutionarily related to components of the bacterial T2SS, although seven of them are so divergent that their evolutionary connection to the T2SS could be recognized only retrospectively after their identification based on their characteristic phylogenetic profile. For the sixteen remaining proteins (Gcp1 to Gcp16) no other obvious evolutionary or functional link to the T2SS is evident apart from the same phyletic pattern as exhibited by the T2SS subunit homologues. Nevertheless, similar phylogenetic profiles are generally a strong indication for proteins being parts of the same functional system or pathway, and have enabled identification of new components of different cellular structures or pathways (e.g. refs [51,52]). Is it, therefore, possible that the 27 Gsp/Gcp proteins similarly belong to a single functional pathway?

The phylogenetic profile shared by the eukaryotic Gsp and Gcp proteins is not trivial, as it implies independent gene losses in a specific set of multiple eukaryotic branches (Fig. 1B). The likelihood of a chance emergence of the same taxonomic distribution of these proteins is thus low. Nevertheless, false positives cannot be completely excluded among the Gcp proteins and their list may be revised when a more comprehensive sampling of eukaryote genomes or transcriptomes becomes available. It is also possible that the currently inferred phylogenetic profile of some of the Gsp/Gcp proteins is incomplete due to limited sampling of the actual gene repertoire of species represented by transcriptome assemblies only. The inherently incomplete nature of single-cell transcriptome assemblies available for hemimastigotes potentially explains our failure to identify homologues of some Gsp and Gcp proteins in this group (Fig. 1B; Supplementary Table 1). An incomplete set is evident also in the heterolobosean *Percolomonas* lineage, as transcriptomic data from three different members revealed only the presence of GspD, GspDL, the three GspDN proteins, and four Gcp proteins (Fig. 1B, Supplementary Table 1). The relatively coherent pattern of Gsp/Gcp protein occurrence in the three independently sequenced transcriptomes and the fact that in other Gsp/Gcp-containing eukaryotes (except for hemimastigotes) all 27 families are always represented in the respective transcriptome assembly (Supplementary Table 1) suggest that the *Percolomonas* lineage has indeed preserved only a subset of Gsp/Gcp families. Genome sequencing is required to test this possibility.

All uncertainties notwithstanding, our data favour the idea that a hitherto unrecognized complex functional pathway exists in some eukaryotic cells, underpinned by most, if not all, of the 27 Gsp/Gcp proteins and possibly others yet to be discovered. Direct biochemical and cell biological investigations are required for testing its existence and the actual cellular role. Nevertheless, we have integrated the experimental data gathered so far with the insights from bioinformatic analyses to propose a hypothetical working model (Fig. 9).

Our main proposition is that the eukaryotic homologues of the bacterial Gsp proteins assemble a functional transport system, here denoted miT2SS, that spans the mitochondrial OM and mediates the export of specific substrate proteins from the mitochondrion. Although the actual architecture of the miT2SS needs to be determined, the available data suggest that it departs in detail from the canonical bacterial T2SS

507 organization, as homologues of some of the important bacterial T2SS components are
508 apparently missing. Most notable is the absence of GspC, presumably related to the
509 modified structure of its interacting partner GspD, which in eukaryotes is split into
510 multiple polypeptides and seems to completely lack the N0 domain involved in GspC
511 binding. It thus remains unclear whether and how the IM assembly platform and the OM
512 pore interact in mitochondria. One possible explanation is that GspC has been replaced
513 by an unrelated protein. It is notable that three Gcp proteins (Gcp7, Gcp11, and Gcp15)
514 have the same general architecture as GspC: they possess a transmembrane segment at
515 the N-terminus and a (predicted) globular domain at the C-terminus (Fig. 9A,
516 Supplementary Fig. 11). Testing possible interactions between these proteins and T2SS
517 core subunits (particularly GspG, GspF and GspDN) using BACTH or Y2H assays will
518 be of future interest.
519 Further investigations also must address the question of whether the
520 mitochondrial GspG is processed analogously to the bacterial homologues and how such
521 processing occurs in the absence of discernible homologues of GspO. The mitochondrial
522 GspG is presumably inserted into the IM by the Tim22 or Tim23 complex, resulting in a
523 GspG precursor with the N-terminus, including the MTS, protruding into the matrix. It is
524 possible that N-terminal cleavage by matrix processing peptidase serves not only to
525 remove the transit peptide, but at the same time to generate the mature N-terminus of the
526 processed GspG form, ready for recruitment into the pseudopilus. A different hypothesis
527 is offered by the discovery of the Gcp16 protein with sequence features suggesting that it
528 is a membrane-embedded metallopeptidase (certainly non-homologous to GspO, which is
529 an aspartic acid peptidase[53]). Although the subcellular localization of Gcp16 needs to be
530 established, we speculate that it might be a mitochondrial IM protein serving as an
531 alternative prepilin peptidase.
532 In parallel with its apparent simplification, the miT2SS may have been
533 specifically elaborated compared to the ancestral bacterial machinery. This possibility is
534 suggested by the existence of two pairs of proteins corresponding to different parts of the
535 bacterial GspE subunit. We propose that the eukaryotic GspE makes a heterodimer with
536 the GspEN2A to reconstitute a unit equivalent to most of the bacterial GspE protein
537 (lacking the GspL-interacting N1E domain), whereas GspEN2B, which is much more
538 divergent from the standard N2E domain than GspEN2A, may pair specifically with
539 GspEL to make an enzymatically inactive GspE-like version. We can only speculate as to
540 the function of these proteins, but the fact that the bacterial GspE assembles into a
541 homohexamer raises the possibility that in eukaryotes catalytically active and inactive
542 versions of GspE are mixed together in a manner analogous to the presence of
543 catalytically active and inactive paralogous subunits in some well-known protein
544 complexes, such as the proton-pumping ATPase (e.g. refs [54,55]). The co-occurrence of two
545 different paralogues of the GspD C-domain, one (GspDL) being particularly divergent,
546 suggests a eukaryote-specific elaboration of the putative pore in the mitochondrial OM.
547 Moreover, the electrophysiology measurements of the pores built of mitochondrial GspD
548 indicated stable complexes of variable sizes; a property not observed for bacterial
549 proteins. Finally, the C-terminal extension of the mitochondrial GspG representing a
550 novel conserved domain without discernible homology to other proteins suggests a
551 eukaryote-specific modification of the pseudopilus functioning.

552 An unanswered key question is what is the actual substrate (or substrates)
553 exported from the mitochondrion by the miT2SS. No bioinformatic tool for T2SS
554 substrate prediction is available due to the enigmatic nature of the mechanism of substrate
555 recognition by the pathway[14], so at the moment we can only speculate. It is notable that
556 no protein encoded by the mitochondrial genomes of jakobids, heteroloboseans and
557 malawimonads stands out as an obvious candidate for the miT2SS substrate, since they
558 either have well-established roles in the mitochondrion or are hypothetical proteins with a
559 restricted (genus-specific) distribution. Therefore, we hypothesize that the substrate is
560 encoded by the nuclear genome and imported into the mitochondrion to undergo a
561 specific processing/maturation step. This may include addition of a prosthetic group – a
562 scenario modelled on the process of cytochrome *c* or Rieske protein maturation[56,57].
563 Interestingly, the proteins Gcp6 and Gcp12, each exhibiting an array of absolutely
564 conserved cysteine and histidine residues (Supplementary Fig. 12), are good candidates
565 for proteins to which a specific prosthetic group might be attached, so any of them may
566 well be the sought-after miT2SS substrate. Some of the other Gcp proteins may then
567 represent components of the hypothetical machinery responsible for the substrate
568 modification. The putative functionalization step may occur either in the mitochondrial
569 matrix or in the intermembrane space (IMS), but we note that the former localization
570 would necessitate a mechanism of protein translocation across the mitochondrial IM in
571 the matrix-to-IMS direction, which has not been demonstrated yet. Regardless, the T2SS
572 system would eventually translocate the modified protein across the mitochondrial OM to
573 the cytoplasm.
574 However, this may not be the end of the journey, since there are hints of a link
575 between the miT2SS-associated pathway and peroxisomes. First, three Gcp proteins,
576 namely Gcp1 to Gcp3, are specifically related to Pex7, a protein mediating import of
577 peroxisomal proteins characterized by the peroxisomal targeting signal 2 (PTS2)[58].
578 Second, some of the Gcp proteins (especially Gcp1 and Gcp13) have at the C-terminus a
579 predicted PTS1 signal (at least in some species; Supplementary Table 1). Third, several
580 Gcp proteins (Gcp2, Gcp9, Gcp10, and Gcp11) and GspEL were assigned to the putative
581 peroxisomal proteome in our proteomic analysis (Supplementary Table 2B). We note the
582 discrepancy between the PTS1 signal predictions and the actual set of experimentally
583 defined peroxisomal proteins, which might be due to an incomplete separation of
584 peroxisome and mitochondria by our purification procedure, but may also reflect protein
585 shuttling between the two organelles. We thus hypothesize that upon its export from the
586 mitochondrion, the miT2SS substrate is eventually delivered to the peroxisome. This is
587 possibly mediated by the Gcp1/2/3 trio, but other Gcp proteins might participate as well.
588 One such protein might be the ubiquitin-related protein Gcp4. Ubiquitination and
589 deubiquitination of several components of the peroxisome protein import machinery are a
590 critical part of the import mechanism[58] and Gcp4 might serve as an analogous peptide
591 modifier in the hypothetical novel peroxisome import pathway functionally linked to the
592 miT2SS.
593 Altogether, our data suggest the existence of a novel elaborate functional
594 pathway combining components of bacterial origin with newly evolved eukaryote-
595 specific proteins. The extant phylogenetic distribution of the pathway is sparse, but our
596 current understanding of eukaryote phylogeny suggests that it was ancestrally present in
597 eukaryotes and for some reason dispensed with multiple times during evolution.

Although we could not define a specific bacterial group as the actual source of the eukaryotic Gsp genes, it is tempting to speculate that the T2SS was introduced into eukaryotes by the bacterial progenitor of mitochondria and that it was involved in delivering specific proteins from the endosymbiont into the host cell, as is known in the case of current intracellular bacteria[59]. Elucidating the actual role of this communication route in establishing the endosymbiont as a fully integrated organelle requires understanding the cellular function of the modern miT2SS-associated pathways, which is a challenge for future research.

Methods

Sequence data and homology searches

Homologues of relevant genes/proteins were searched in sequence databases accessible via the National Center for Biotechnology Information BLAST server (https://blast.ncbi.nlm.nih.gov/Blast.cgi), including the nucleotide and protein non-redundant (nr) databases, whole-genome shotgun assemblies (WGAs), expressed sequence tags (ESTs), and transcriptome shotgun assemblies (TSAs). Additional public databases searched included the data provided by the Marine Microbial Eukaryote Transcriptome Sequencing Project (MMETSP[60]) comprising TSAs from hundreds of diverse protists (https://www.imicrobe.us/#/projects/104), the OneKP project[61] (https://sites.google.com/a/ualberta.ca/onekp/) comprising TSAs from hundreds of plants and algae, and individual WGAs and TSAs deposited at various on-line repositories (Supplementary Table 4). To further improve the sampling, draft genome assemblies were generated in this study for the heterolobosean *Neovahlkampfia damariscottae* and the malawimonad informally called "*Malawimonas californiana*". Details on the sequencing and assembly are provided in Supplementary Methods. Finally, the analyses also included sequence data from genome and/or transcriptome projects for several protists that are underway in our laboratories and will be published in full elsewhere upon completion (Supplementary Table 4). Relevant sequences were extracted from these unpublished datasets and either deposited in GenBank or included in Supplementary Table 1.

Similarity searches were done using BLAST[62] (blastp or tblastn, depending on the database queried) and HMMER[63] using profile HMMs built from sequence alignments of proteins of interest. Hits were evaluated by BLAST (blastp or blastx) searches against the nr protein dataset at NCBI to distinguish orthologues of Gsp and Gcp proteins from paralogous proteins or non-specific matches. This was facilitated by a high degree of conservation of individual eukaryotic Gsp/Gcp proteins among different species (see also Supplementary Figs 4 and 11-13) and in most cases by the lack of other close homologues in eukaryotic genomes (the exceptions being members of broader protein families, including the ATPase GspE, the WD40 superfamily proteins Gcp1 to Gcp3, and the ubiquitin-related protein Gcp4). All identified eukaryotic Gsp and Gcp sequences were carefully manually curated to ensure maximal accuracy and completeness of the data, which included correction of existing gene models, extension of truncated sequences by manual analysis of raw sequencing reads, and correction of assembly errors (for details see Supplementary Methods). All newly predicted or curated Gsp and Gcp sequences are provided in Supplementary Table 1; additional Gsp and Gcp sequences from non-target species are listed in Supplementary Table 4. The nomenclature of the

Gsp and Gcp genes proposed in this study was also reflected in the annotation of the *A. godoyi* genome, recently published as part of a separate study[5].

Phylogenetic profiling

In order to identify genes with the same phylogenetic distribution as the eukaryotic homologues of the four core T2SS components, we carried out two partially overlapping analyses based on defining groups of putative orthologous genes in select Gsp-positive species and phylogenetically diverse Gsp-negative eukaryotic species. The list of taxa included is provided in Supplementary Table 5. The first analysis was based on 18 species, including three Gsp-positive ones (*N. gruberi*, *A. godoyi* and *M. jakobiformis*), for the second analysis the set was expanded by adding one additional Gsp-positive species (*G. okellyi*) and one Gsp-negative species (*Monocercomonoides exilis*). Briefly, the protein sequences of a given species were compared to those of all other species using blastp followed by fast phylogenetic analyses, and orthologous relationships between proteins were then inferred from this set of phylogenetic trees using a reference-species-tree-independent approach. This procedure was repeated for each species and all resulting sets of orthologous relationships, also known as phylomes[64], were combined in a dense network of orthologous relationships. This network was finally trimmed in several successive steps to remove weak or spurious connections and to account for (genuine or artificial) gene fusions, with the first analysis being less restrictive than the second. Details of this pipeline are provided in Supplementary Methods. For each of the two analyses, the final set of defined groups of orthologs (orthogroups) was parsed to identify those comprising genes from at least two Gsp-positive species yet lacking genes from any Gsp-negative species. The orthogroups passing this criterion were further analysed manually by blastp and tblastn searches against various public and private sequence repositories (see the section "Sequence data and homology searches") to exclude those orthogroups with obvious orthologs in Gsp-negative species. *Percolomonas* lineage exhibiting only GspD and jakobids represented by incomplete EST surveys (these species likely possess the miT2SS system) were not considered Gsp-negative. The orthogroups that remained were then evaluated for their conservation in Gsp-positive species and those that proved to have a representative in all these species (*N. gruberi*, *N. fowleri*, *N. damariscottae*, *P. kirbyi*, *A. godoyi*, *R. americana*, *M. jakobiformis*, *G. okellyi*) were considered as bona fide Gcp (Gsp-co-occurring protein) candidates. It is of note that some of these proteins are short and were missed by the automated annotation of some of the genomes, so using relaxed criteria for the initial consideration of candidate orthogroups (i.e. allowing for their absence from some of the Gsp-positive species) proved critical for decreasing the number of false-negative identifications.

Sequence analyses and phylogenetic inference

Subcellular targeting of Gsp and Gcp proteins was evaluated using TargetP-1.1 (ref. [65]; http://www.cbs.dtu.dk/services/TargetP-1.1/index.php), TargetP-2.0 (ref. [66]; http://www.cbs.dtu.dk/services/TargetP/), Mitoprot II (ref. [67]; https://ihg.gsf.de/ihg/mitoprot.html), MitoFates[68] (http://mitf.cbrc.jp/MitoFates/cgi-bin/top.cgi)[68], WoLF PSORT (https://wolfpsort.hgc.jp/), and PTS1 predictor[69] (http://mendel.imp.ac.at/pts1/). Transmembrane domains were predicted using TMHMM[70] (http://www.cbs.dtu.dk/services/TMHMM/). Homology of Gsp and Gcp

690 protein families to other proteins was evaluated by searches against Pfam v. 31 (ref. [71];
691 http://pfam.xfam.org/) and Superfamily 1.75 database[72]
692 (http://supfam.org/SUPERFAMILY/index.html), and by using HHpred[45]
693 (https://toolkit.tuebingen.mpg.de/#/tools/hhpred) and the Phyre2 server[46]
694 (http://www.sbg.bio.ic.ac.uk/phyre2/html/page.cgi?id=index). The relative position of the
695 Gcp4 family among ubiquitin-like proteins was analysed by a cluster analysis using
696 CLANS[73] (https://www.eb.tuebingen.mpg.de/protein-evolution/software/clans/); for the
697 analysis the Gcp4 family was combined with all 59 defined families included in the clan
698 Ubiquitin (CL0072) as defined in the Pfam database (each family was represented by
699 sequences from the respective seed alignments stored in the Pfam database). For further
700 details on the procedure see the legend of Supplementary Fig. 10A. Multiple sequence
701 alignments used for presentation of the conservation and specific sequence features of
702 Gsp and Gcp families were built using MUSCLE[74] and shaded using BioEdit
703 (http://www.mbio.ncsu.edu/BioEdit/bioedit.html).
704 In order to obtain datasets for the phylogenetic analyses of eukaryotic GspD to
705 GspG proteins, the protein sequences were aligned using MAFFT[75] and trimmed
706 manually. Profile hidden Markov models (HMMs) built on the basis of the respective
707 alignments were used as queries to search the UniProt database using HMMER. All
708 recovered sequences were assigned to components of the T4P superfamily machineries
709 using HMMER searches against a collection of profile HMMs reported by Abby et al.
710 (ref. [76]). For each GspD to GspG proteins, a series of alignments was built by
711 progressively expanding the sequence set by including more distant homologues (as
712 retrieved by the HMMER searches). Specifically, the different sets of sequences were
713 defined by the HMMER score based on the formula $score_{cutoff} = c*score_{best\ prokaryotic\ hit}$,
714 with the coefficient c decreasing from 0.99 to 0.70 incrementally by 0.01. The sequences
715 were then aligned using MAFFT, trimmed with BMGE[77] and the phylogenies were
716 computed with IQ-TREE[78] using the best-fit model (selected by the program from
717 standard protein evolution models and the mixture models[79] offered). The topologies
718 were tested using 10,000 ultra-fast bootstraps. The resulting trees were systematically
719 analyzed for support of the monophyly of eukaryotic sequences and for the taxonomic
720 assignment of the parental prokaryotic node of the eukaryotic subtree. The assignment
721 was done using the following procedure. The tree was artificially rooted between the
722 eukaryotic and prokaryotic sequences. From sub-leaf nodes to the deepest node of the
723 prokaryotic subtree, the taxonomic affiliation of each node was assigned by
724 proportionally considering the known or inferred taxonomic affiliations (at the phylum or
725 class level) of the descending nodes. See the legend to Supplementary Fig. 3 for further
726 details.
727 The phylogenetic analysis of the WD40 superfamily including Gcp1 to Gcp3
728 proteins was performed as follows. The starting dataset was prepared by a combination of
729 two different approaches: 1) each identified sequence of Gcp1 to Gcp3 proteins was used
730 as a query in a blastp search against the non-redundant (nr) NCBI protein database and
731 the 500 best hits for each sequence were kept; 2) protein sequences of each the Gcp1 to
732 Gcp3 family were aligned using MAFFT and the multiple alignment was used as a query
733 in a HMMER3 search (https://toolkit.tuebingen.mpg.de/#/tools/hmmer) against the
734 UniProt database. Best hits (E-value cutoff 1e-50) from the two searches were pooled and
735 de-duplicated, and the resulting sequence set (including Gcp1 to Gcp3 sequences) was

aligned using MAFFT and trimmed manually to remove poorly conserved regions. Because WD40 proteins are extremely diversified, sequences that were too divergent were eliminated from the starting dataset during three subsequent rounds of sequence removal, based on a manual inspection of the alignment and phylogenetic trees computed by IQ-TREE (using the best-fit model as described above). The final dataset was enriched by adding PEX7 and WDR24 orthologues from eukaryotes known to possess miT2SS components. The final phylogenetic tree was computed using IQ-TEE as described in the legend to Supplementary Fig. 9. IQ-TREE was used also for inferring trees of the heterolobosean 18S rRNA gene sequences (Supplementary Fig. 1), ubiquitin-related proteins (Supplementary Fig. 10B) and the Gcp16 family (Supplementary Fig. 14); details on the analyses are provided in legends to the respective figures.

Structural homology modelling

The PDB database was searched by the SWISS-MODEL server[80] for structural homologues of *Go*GspD and *Go*GspG1. *V. cholerae* GspD[20] (PDB entry 5WQ9) and *K. oxytoca* PulG[47] pseudopilus (PDB entry 5WDA) were selected as the top matches, respectively. Models were built based on the target-template alignment using ProMod3 (ref. [80]). Coordinates that were conserved between the target and the template were copied from the template to the model. Insertions and deletions were remodelled using a fragment library, followed by rebuilding side chains. Finally, the geometry of the resulting model was regularized by using a force field. In the case of loop modelling with ProMod3 fails, an alternative model was built with PROMOD-II (ref. [81]). The quaternary structure annotation of the template was used to model the target sequence in its oligomeric form[82].

Cultivation and fractionation of *N. gruberi* and proteomic analysis

Naegleria gruberi str. NEG-M was axenically cultured in M7 medium with PenStrep (100 U/mL of penicillin and 100 µg/mL of streptomycin) at 27°C in vented tissue culture flasks. Mitochondria of *N. gruberi* were isolated in seven independent experiments and were analyzed individually (see below). Each time ~1×10^9 *N. gruberi* cells were resuspended in 2 mL of SM buffer (250 mM sucrose, 20 mM MOPS, pH 7.4) supplemented with DNase I (40 µg/mL) and Roche cOmplete™ EDTA-free Protease Inhibitor Cocktail and homogenized by eight passages through a 33-gauge hypodermic needle (Sigma Aldrich). The resulting cell homogenate was then cleaned of cellular debris using differential centrifugation and separated by a 2-hr centrifugation in a discontinuous density OptiPrep gradient (10%, 15%, 20%, 30% and 50%) as described previously[83]. Three visually identifiable fractions corresponding to 10-15% (OPT-1015), 15-20% (OPT-1520) and 20-30% (OPT-2023) OptiPrep densities were collected (each in five biological replicates) and washed with SM buffer.

Proteins extracted from these samples were then digested with trypsin and peptides were separated by nanoflow liquid chromatography and analyzed by tandem mass spectrometry (nLC-MS2) on a Thermo Orbitrap Fusion (q-OT-IT) instrument as described elsewhere[84]. The quantification of mass spectrometry data in the MaxQuant software[85] provided normalized intensity values for 4,198 proteins in all samples and all three fractions. These values were further processed using the Perseus software[86]. Data were filtered and only proteins with at least two valid values in one fraction were kept.

Imputation of missing values, which represent low-abundance measurements, was performed with random distribution around the value of instrument sensitivity using default settings of Perseus software[86].

The data were analyzed by principle component analysis (PCA). The first two loadings of the PCA were used to plot a two-dimensional graph. Based on a set of marker proteins (376 mitochondrial and 26 peroxisomal, Supplementary Table 2), clusters of proteins co-fractionating with mitochondria and peroxisomes were defined and the proteins within the clusters were further analyzed. This workflow was set up on the basis of the LOPIT protocol[87]. As a result, out of the 4,198 proteins detected, 946 putative mitochondrial and 78 putative peroxisomal proteins were defined. All proteins were subjected to *in silico* predictions concerning their function (BLAST, HHpred[45]) and subcellular localization (Psort II, https://psort.hgc.jp/form2.html; TargetP, http://www.cbs.dtu.dk/services/TargetP/; MultiLoc2, https://abi.inf.uni-tuebingen.de/Services/MultiLoc2).

Fluorescence *in situ* hybridization (FISH)

The PCR products of the *NgGspE* and *NgGspF* genes were labelled by alkali-stable digoxigenin-11-dUTP (Roche) using DecaLabel DNA Labeling Kit (Thermo Scientific). Labelled probes were purified on columns of QIAquick Gel Extraction Kit (Qiagen, 28704) in a final volume of 50 µL. Labelling efficiencies were tested by dot blotting with anti-digoxigenin alkaline phosphatase conjugate and CSPD chemiluminescence substrate for alkaline phosphatase from DIG High Prime DNA Labelling and Detection Starter Kit II (Roche) according to the manufacturer`s protocol. FISH with digoxigenin-labelled probes was performed essentially according to the procedure described in Zubacova at al.[88] with some modifications. *N. gruberi* cells were pelleted by centrifugation for 10 min at 2,000 × g at 4°C. Cells were placed in hypotonic solution, fixed twice with a freshly prepared mixture of methanol and acetic acid (3:1) and dropped on superfrost microscope slides (ThermoScientific). Preparations for hybridizations were treated with RNase A, 20 µg in 100 µL 2 × SSC, for 1 hr at 37°C, washed twice in 2 × SSC for 5 min, dehydrated in a methanol series and air-dried. Slides were treated with 50% acetic acid followed by pepsin treatment and postfixation with 2% paraformaldehyde. Endogenous peroxidase activity of the cell remnants (undesirable for tyramide signal amplification) was inactivated by incubation in 1% hydrogen peroxide, followed by dehydration in a graded methanol series. All slides were denatured together with 2 µL (25 ng) of the probe in 50 µL of hybridization mixture containing 50% deionised formamide (Sigma) in 2 × SSC for 5 min at 82°C. Hybridizations were carried out overnight. Slides were incubated with tyramide reagent for 7 min. Preparations were counterstained with DAPI in VectaShield and observed under an Olympus IX81 microscope equipped with a Hamamatsu Orca-AG digital camera using the Cell^R imaging software.

Heterologous gene expression, preparation of antibodies

The selected Gsp genes from *G. okellyi* and *N. gruberi* were amplified from commercially synthesized templates (Genscript; for primers used for PCR amplification of the coding sequences see Supplementary Table 6) and cloned into the pUG35 vector. The constructs were introduced into *S. cerevisiae* strain YPH499 by the lithium acetate/PEG method. The positive colonies grown on SD-URA plates were incubated

with MitoTracker Red CMXRos (Thermo Fisher Scientific) and observed for GFP and MitoTracker fluorescence (using the same equipment as used for FISH, see above). For the expression in *T. brucei,* sequences encoding full-length *Go*GspD, *Go*GspG2, *Ng*GspG1 as well as the first 160 amino acid residues from *Ng*GspG1 were amplified from the commercially synthesized templates and cloned into the pT7 plasmid, encoding either three C-terminal V5 tags (full-length genes) or C-terminal mNeonGreen followed by three V5 tags (*Ng*GspG1 targeting sequence). *T. brucei* cell line SMOX 927 (ref. [89]) were grown in SDM79 media[90] supplemented with 10% fetal bovine serum (Gibco). *NotI*-linearized plasmids (50 µg) were nucleofected into procyclic *T. brucei* cells using an Amaxa nucleofector (Lonza) as described before[91]. Expression of the genes was induced by an overnight incubation with doxycycline (1 µg/ml). For bacterial expression, genes encoding *Ng*GspG1 and *Ng*GspEN2A were amplified from commercially synthesized templates and cloned into the pET42b vector (for primers used for PCR amplification of the coding sequences, see Supplementary Table 6). The constructs were introduced into the chemically-competent *E. coli* strain BL21(DE3) and their expression induced by 1 mM IPTG. The recombinant proteins were purified under denaturing conditions on Ni-NTA agarose (Qiagen). The purified proteins were used for rat immunization in an in-house animal facility at the Charles University.

Immunofluorescence microscopy

Yeast, procyclic *T. brucei* or *N. gruberi* cells were pre-treated by incubation with MitoTracker CMX Ros (1:000 dilution) for 20 min to stain mitochondria, washed twice in PBS and placed on coverslips. After a 5-min incubation, the cells were fixed with 4% PFA in PBS for 15 min. The solution was replaced by 0.1% Triton X-100 in PBS and the slides were incubated for 15 min. The slides were then treated with blocking buffer (1% BSA and 0.033% Triton X-100 in PBS) for 1 hr at room temperature. After blocking, the samples were stained overnight at 4°C with a blocking solution supplemented with the primary antibody (in-house-produced rat anti-*Ng*GspG1 and anti-*Ng*GspEN2A antibodies, dilutions 1:100, rat anti-V5 antibody Abcam, dilution 1:1000 dilution). The slides were washed three times for 10 min with 0.033% Triton X-100 and incubated with an anti-rat antibody conjugated with Alexa Fluor® 488 (1:1000 dilution, Thermo Fisher Scientific) in blocking buffer for 1 hr at room temperature. Slides were washed twice in PBS supplemented with 0.033% Triton X-100 for 10 min followed by a single 10-min wash with PBS only. The slides were mounted in Vectashield containing DAPI (Vector laboratories). Static images were acquired on a Leica SP8 FLIM inverted confocal microscope equipped with 405 nm and white light (470-670 nm) lasers and a FOV SP8 scanner using an HC PL APO CS2 63x/1.4 NA oil-immersion objective. Laser wavelengths and intensities were controlled by a combination of AOTF and AOBS separately for each channel. Emitting fluorescence was captured by internal spectrally-tunable HyD detectors. Imaging was controlled by the Leica LAS-X software. Images were deconvolved using the SVI Huygens Professional software (Scientific Volume Imaging) with the CMLE algorithm. Maximum intensity projections and brightness/contrast corrections were performed in the FIJI ImageJ software.

Purification of native *Ng*GspD and *Ng*GspG

His-tagged *Ng*GspD carrying the signal peptide of *E. coli* DsbA was produced in the *E. coli* strain BL21 (DE3) in auto-induction media (50 mM Na_2HPO_4, 50 mM KH_2PO_4, 2% Tryptone, 0.5% Yeast extract, 85 mM NaCl, 0.5% glycerol, 0.05% glucose and 0.2% lactose) as described in ref. [92]. The cells were grown at 37°C for 16 hr, centrifuged at 6,000 × g for 15 min at 4°C and resuspended in 20 mM Tris pH 8, 5 mM EDTA. Bacteria were incubated for 30 min on ice in the presence of lysozyme (1 mg/ml) and DNAse, and lysed in a French press. The cell lysate was centrifuged at 6,000 × g for 15 min at 4°C to pellet cell debris. The cleared lysate was then centrifuged at 100,000 × g for 2 h at 4°C and membrane pellet was washed twice in 20 mM Tris pH 8, with 1-hr centrifugation steps (100,000 × g at 4°C). The membranes were resuspended to the final protein concentration of 1 mg/ml in 50 mM Tris pH 8, 250 mM NaCl, 1% Zwittergent 3-14, and solubilized for 2 hr at 4°C. The sample was then centrifuged at 100,000 × g for 1 hr at 4°C. His-tagged proteins from the supernatant were incubated overnight with Ni-NTA agarose (Qiagen) at 4°C. The next day, the agarose was collected on a column and washed with 50 ml of 50 mM Tris pH 8, 250 mM NaCl, 20 mM Imidazole, 0.5% Zwittergent 3-14. Bound proteins were eluted by 5 × 0.5 ml of 50 mM Tris pH 8, 250 mM NaCl, 250 mM imidazole, Zwittergent 3-14. Collected fractions were analyzed by SDS PAGE and western blotting. Selected samples were then pooled together, re-buffered into 50 mM Tris pH 8, 250 mM NaCl, 0.5% Zwittergent 3-14, and analyzed by size exclusion chromatography.

For *Ng*GspG1, the BL21 cells expressing the pseudopilin domain lacking the N-terminal hydrophobic part were collected after 4 hr of IPTG induction at 37°C. The cells were collected, washed with PBS, and then resuspended in 35 ml of 50 mM Tris, 100 mM NaCl, pH 8 with added inhibitors (cOMPLETE™ tablets, EDTA-free, Roche), DNAse (1 mg/ml), 5 mM $MgCl_2$ and lysozyme (1 mg/ml). The suspension was incubated on ice for 30 min. After lysis via French press the resulting suspension was spun down for 20 min at 100,000 × g, 4 °C. Ni-NTA agarose beads (1 ml; Qiagen), washed and resuspended in loading buffer (50 mM Tris, 100 mM NaCl, 10 mM imidazole, pH 8), were added to the supernatant. The supernatant was incubated with the beads for 1 hr on a tube rotator at 4°C. The suspension was then applied to a column. The beads on the column were then washed with 8 ml of wash buffer (50mM Tris, 100 mM NaCl, 20 mM imidazole, pH 8). The protein was eluted by 4 ml elution buffer I (50 mM Tris, 100 mM NaCl, 100 mM imidazole, pH 8) and 4 ml of elution buffer II (50 mM Tris, 100 mM NaCl, 150 mM imidazole, pH 8). All elutions were then rebuffered to 50 mM Tris pH 8, 100 mM NaCl, using Amicon Ultra-4 10k centrifugal filter tubes. The protein binding was measured by the microscale thermophoresis technique on a Monolith NT.115 instrument (Nanotemper). Protein (10 nM) in 50 mM HEPES buffer with 50 mM NaCl was labelled with Red-NHS dye NT-647. Maximum concentration of titrated protein was 50 μM.

Black lipid membrane measurements

Planar lipid membrane experiments were performed as described previously[93]. The electrolyte solution contained 1 M KCl and 10 mM Tris-HCl (pH 7.4). 5 μl of purified protein (80 ng/ml) was mixed with 1500 μl KCl and was added to the *cis* compartment with a positive electrode, whereas the *trans* compartment was grounded. Planar lipid membrane was formed across a 0.5-mm aperture by painting the *E. coli* polar lipids

extract (3% wt/vol, Avanti Polar Lipids, Alabaster, USA) dissolved in *n*-decan and butanol (9:1). The membrane current was registered using Ag/AgCl electrodes with salt bridges connected to an LCA-200-10G amplifier (Femto, Germany) and digitized with a KPCI-3108 16-Bit A/D card (Keithley Instruments, USA) with a 1-kHz sampling rate. Single-pore recordings were processed in the program QuB[94]. The histogram of single-pore conductance (n=100) was constructed by kernel density estimation (with the Gaussian kernel of 100-pS width) to overcome bin edge effects.

In vitro protein translation and mitochondrial protein import

The *Go*GspD and *Ng*GspD genes were amplified from commercially synthesized templates (for primers used for PCR amplification of the coding sequences, see Supplementary Table 6) and cloned into pDHFR vector provided in the PURExpress *In Vitro* Protein Synthesis Kit (NEB). The translation into liposomes was done as described previously[95] and the output was analyzed by Blue Native PAGE using 2% digitonin and NativePAGE Novex 4-16% Bis-Tris Protein Gel (Thermo Fisher Scientific). For the *in vitro* mitochondrial protein import, the mitochondria were isolated from *S. cerevisiae* YPH499 according to the method described in ref. [96]. The *in vitro*-translated *Go*GspD and Su9-DHFR chimeric construct[41] were incubated with mitochondria as described in ref. [97].

Testing protein interactions using two-hybrid systems

Bacterial two-hybrid system (BACTH) analysis was performed as described before[98]. Gsp genes were amplified with specific primers (listed in Supplementary Table 6) and cloned into pKT25 and pUT18c plasmids. *E. coli* strain DHT1 competent cells were co-transformed with two plasmids with different combinations of Gsp genes. Co-transformants were selected on LB plates with ampicillin (Ap) (100 µg/mL) and kanamycin (Km) (25 µg/mL). Colonies were grown at 30°C for 48 to 96 hr. From each plate three colonies were picked, transferred to 1 mL of LB medium with Ap and Km, and grown overnight at 30°C with shaking. Next day, precultures (0.25 mL) were inoculated to 5 mL of LB medium with Ap, Km and 1 mM IPTG. Cultures were grown with shaking at 30°C to OD_{600} of about 1-1.5. Bacteria (0.5 mL) were mixed with 0.5 mL of Z buffer and β-galactosidase activity was measured[99].

The yeast two-hybrid system (Y2H) was employed as described in ref. [100]. Cells of *S. cerevisiae* strain AH109 were co-transformed with two plasmids (pGADT7, pGBKT7) with different combinations of Gsp genes. Co-transformants were selected on double-dropout SD-Leu/-Trp and triple-dropout SD-Leu/-Trp/-His plates. The colonies were grown for a few days. Positive colonies from the triple dropout were grown overnight at 30°C with shaking and then the serial dilution test was performed on double- and triple-dropout plates.

Data availability

All sequences of Gsp and Gcp proteins analysed in the study are provided in Supplementary Table 1. Gsp and Gcp genes extracted from an unpublished *Malawimonas jakobiformis* genome assembly have been deposited at GenBank with accession numbers MT460910-MT460938. Raw genome sequencing reads from "*Malawimonas californiana*" and *Neovahlkampfia damariscottae* are available from NCBI under the BioProject PRJNA549687. The genome assembly of *N. damariscottae* has been

deposited at GenBank with the accession number JABLTG000000000. The transcriptome assembly of *Gefionella okellyi*, the genome assembly and predicted proteins of "*Malawimonas californiana*", and partial genome assemblies of *Reclinomonas americana* are available from https://megasun.bch.umontreal.ca/papers/T2SS-2020/. The mass spectrometry proteomics data have been deposited in the ProteomeXchange Consortium via the PRIDE[101] partner repository with the dataset identifier PXD007764. Other relevant data (e.g. multiple sequence alignments used for phylogenetic analyses) are available from the authors upon request.

References

1. Roger, A. J., Muñoz-Gómez, S. A. & Kamikawa, R. The origin and diversification of mitochondria. *Curr. Biol.* **27**, R1177–R1192 (2017).
2. Martijn, J., Vosseberg, J., Guy, L., Offre, P. & Ettema, T. J. G. Deep mitochondrial origin outside the sampled alphaproteobacteria. *Nature* **557**, 101–105 (2018).
3. Leger, M. M. *et al.* An ancestral bacterial division system is widespread in eukaryotic mitochondria. *Proc. Natl. Acad. Sci. U. S. A.* **112**, 10239–46 (2015).
4. Beech, P. L. Mitochondrial FtsZ in a chromophyte alga. *Science* **287**, 1276–1279 (2000).
5. Gray, M. W. *et al.* The draft nuclear genome sequence and predicted mitochondrial proteome of Andalucia godoyi, a protist with the most gene-rich and bacteria-like mitochondrial genome. *BMC Biol.* **18**, (2020).
6. Natale, P., Brüser, T. & Driessen, A. J. M. Sec- and Tat-mediated protein secretion across the bacterial cytoplasmic membrane—Distinct translocases and mechanisms. *Biochim. Biophys. Acta - Biomembr.* **1778**, 1735–1756 (2008).
7. Costa, T. R. D. *et al.* Secretion systems in Gram-negative bacteria: structural and mechanistic insights. *Nat. Rev. Microbiol.* **13**, 343–359 (2015).
8. Dolezal, P., Likic, V., Tachezy, J. & Lithgow, T. Evolution of the molecular machines for protein import into mitochondria. *Science* **313**, 314–8 (2006).
9. Petru, M. *et al.* Evolution of mitochondrial TAT translocases illustrates the loss of bacterial protein transport machines in mitochondria. *BMC Biol.* **16**, (2018).
10. Schäfer, K., Künzler, P., Klingl, A., Eubel, H. & Carrie, C. The plant mitochondrial TAT pathway is essential for complex III biogenesis. *Curr. Biol.* **30**, 840-853.e5 (2020).
11. Lang, B. F. *et al.* An ancestral mitochondrial DNA resembling a eubacterial genome in miniature. *Nature* **387**, 493–7 (1997).
12. Burger, G., Gray, M. W., Forget, L. & Lang, B. F. Strikingly bacteria-like and gene-rich mitochondrial genomes throughout jakobid protists. *Genome Biol. Evol.* **5**, 418–38 (2013).
13. Tong, J. *et al.* Ancestral and derived protein import pathways in the mitochondrion of *Reclinomonas america*. *Mol. Biol. Evol.* **28**, 1581–91 (2011).
14. Korotkov, K. V., Sandkvist, M. & Hol, W. G. J. The type II secretion system: biogenesis, molecular architecture and mechanism. *Nat. Rev. Microbiol.* **10**, 336–51 (2012).
15. Thomassin, J.-L., Santos Moreno, J., Guilvout, I., Tran Van Nhieu, G. & Francetic, O. The trans-envelope architecture and function of the type 2 secretion system:

1011 new insights raising new questions. *Mol. Microbiol.* **105**, 211–226 (2017).
1012 16. Berry, J.-L. & Pelicic, V. Exceptionally widespread nanomachines composed of
1013 type IV pilins: the prokaryotic Swiss Army knives. *FEMS Microbiol. Rev.* **39**,
1014 134–54 (2015).
1015 17. Nivaskumar, M. & Francetic, O. Type II secretion system: a magic beanstalk or a
1016 protein escalator. *Biochim. Biophys. Acta* **1843**, 1568–77 (2014).
1017 18. Denise, R., Abby, S. S. & Rocha, E. P. C. Diversification of the type IV filament
1018 superfamily into machines for adhesion, protein secretion, DNA uptake, and
1019 motility. *PLoS Biol.* **17**, e3000390 (2019).
1020 19. Guilvout, I. *et al.* In vitro multimerization and membrane insertion of bacterial
1021 outer membrane secretin PulD. *J. Mol. Biol.* **382**, 13–23 (2008).
1022 20. Yan, Z., Yin, M., Xu, D., Zhu, Y. & Li, X. Structural insights into the secretin
1023 translocation channel in the type II secretion system. *Nat. Struct. Mol. Biol.* **24**,
1024 177–183 (2017).
1025 21. Py, B., Loiseau, L. & Barras, F. An inner membrane platform in the type II
1026 secretion machinery of Gram-negative bacteria. *EMBO Rep.* **2**, 244–248 (2001).
1027 22. Wang, X. *et al.* Cysteine scanning mutagenesis and disulfide mapping analysis of
1028 arrangement of GspC and GspD protomers within the type 2 secretion system. *J.*
1029 *Biol. Chem.* **287**, 19082–93 (2012).
1030 23. Korotkov, K. V. *et al.* Structural and functional studies on the interaction of GspC
1031 and GspD in the type II secretion system. *PLoS Pathog.* **7**, e1002228 (2011).
1032 24. Korotkov, K. V & Hol, W. G. J. Structure of the GspK-GspI-GspJ complex from
1033 the enterotoxigenic Escherichia coli type 2 secretion system. *Nat. Struct. Mol. Biol.*
1034 **15**, 462–8 (2008).
1035 25. Peabody, C. R. *et al.* Type II protein secretion and its relationship to bacterial type
1036 IV pili and archaeal flagella. *Microbiology* **149**, 3051–72 (2003).
1037 26. Lu, C. *et al.* Hexamers of the type II secretion ATPase GspE from Vibrio cholerae
1038 with Increased ATPase activity. *Structure* **21**, 1707–1717 (2013).
1039 27. Lax, G. *et al.* Hemimastigophora is a novel supra-kingdom-level lineage of
1040 eukaryotes. *Nature* **564**, 410–414 (2018).
1041 28. Adl, S. M. *et al.* The revised classification of eukaryotes. *J. Eukaryot. Microbiol.*
1042 **59**, 429–514 (2012).
1043 29. Derelle, R. *et al.* Bacterial proteins pinpoint a single eukaryotic root. *Proc. Natl.*
1044 *Acad. Sci. U. S. A.* **112**, E693-9 (2015).
1045 30. Karnkowska, A. *et al.* A eukaryote without a mitochondrial organelle. *Curr. Biol.*
1046 **26**, 1274–84 (2016).
1047 31. Heiss, A. A. *et al.* Combined morphological and phylogenomic re-examination of
1048 malawimonads, a critical taxon for inferring the evolutionary history of
1049 eukaryotes. *R. Soc. Open Sci.* **5**, 171707 (2018).
1050 32. Brown, M. W. *et al.* Phylogenomics places orphan protistan lineages in a novel
1051 eukaryotic super-group. *Genome Biol. Evol.* **10**, 427–433 (2018).
1052 33. Mach, J. *et al.* Iron economy in *Naegleria gruberi* reflects its metabolic flexibility.
1053 *Int. J. Parasitol.* **48**, 719–727 (2018).
1054 34. Nouwen, N. *et al.* Secretin PulD: Association with pilot PulS, structure, and ion-
1055 conducting channel formation. *Proc. Natl. Acad. Sci.* **96**, 8173–8177 (1999).
1056 35. Hardie, K. R., Lory, S. & Pugsley, A. P. Insertion of an outer membrane protein in

1057 *Escherichia coli* requires a chaperone-like protein. *EMBO J.* **15**, 978–88 (1996).
1058 36. Dunstan, R. A. *et al.* Assembly of the secretion pores GspD, Wza and CsgG into
1059 bacterial outer membranes does not require the Omp85 proteins BamA or TamA.
1060 *Mol. Microbiol.* **97**, 616–629 (2015).
1061 37. Collin, S., Guilvout, I., Chami, M. & Pugsley, A. P. YaeT-independent
1062 multimerization and outer membrane association of secretin PulD. *Mol. Microbiol.*
1063 **64**, 1350–1357 (2007).
1064 38. Korotkov, K. V, Pardon, E., Steyaert, J. & Hol, W. G. J. Crystal structure of the N-
1065 terminal domain of the secretin GspD from ETEC determined with the assistance
1066 of a nanobody. *Structure* **17**, 255–265 (2009).
1067 39. Guilvout, I. *et al.* Prepore stability controls productive folding of the BAM
1068 independent multimeric outer membrane secretin PulD. *J. Biol. Chem.* **292**, 328–
1069 338 (2017).
1070 40. Chernyatina, A. A. & Low, H. H. Core architecture of a bacterial type II secretion
1071 system. *Nat. Commun.* **10**, 5437 (2019).
1072 41. Pfanner, N., Tropschug, M. & Neupert, W. Mitochondrial protein import:
1073 Nucleoside triphosphates are involved in conferring import-competence to
1074 precursors. *Cell* **49**, 815–823 (1987).
1075 42. Yin, M., Yan, Z. & Li, X. Structural insight into the assembly of the Type II
1076 secretion system pilotin-Secretin complex from enterotoxigenic *Escherichia coli*.
1077 *Nat Microbiol* (2018). doi:10.2210/PDB5ZDH/PDB
1078 43. Guilvout, I. *et al.* In Vitro Multimerization and Membrane Insertion of Bacterial
1079 Outer Membrane Secretin PulD. *J. Mol. Biol.* **382**, 13–23 (2008).
1080 44. Sauvonnet, N., Vignon, G., Pugsley, A. P. & Gounon, P. Pilus formation and
1081 protein secretion by the same machinery in Escherichia coli. *EMBO J.* **19**, 2221–
1082 2228 (2000).
1083 45. Alva, V., Nam, S.-Z., Söding, J. & Lupas, A. N. The MPI bioinformatics Toolkit
1084 as an integrative platform for advanced protein sequence and structure analysis.
1085 *Nucleic Acids Res.* **44**, W410–W415 (2016).
1086 46. Kelley, L. A., Mezulis, S., Yates, C. M., Wass, M. N. & Sternberg, M. J. E. The
1087 Phyre2 web portal for protein modeling, prediction and analysis. *Nat. Protoc.* **10**,
1088 845–858 (2015).
1089 47. López-Castilla, A. *et al.* Structure of the calcium-dependent type 2 secretion
1090 pseudopilus. *Nat. Microbiol.* **2**, 1686–1695 (2017).
1091 48. Nivaskumar, M. *et al.* Pseudopilin residue E5 is essential for recruitment by the
1092 type 2 secretion system assembly platform. *Mol. Microbiol.* **101**, 924–41 (2016).
1093 49. Lu, C., Korotkov, K. V. & Hol, W. G. J. Crystal structure of the full-length
1094 ATPase GspE from the Vibrio vulnificus type II secretion system in complex with
1095 the cytoplasmic domain of GspL. *J. Struct. Biol.* **187**, 223–235 (2014).
1096 50. Cerdà-Costa, N. & Xavier Gomis-Rüth, F. Architecture and function of
1097 metallopeptidase catalytic domains. *Protein Sci.* **23**, 123–144 (2014).
1098 51. Tabach, Y. *et al.* Identification of small RNA pathway genes using patterns of
1099 phylogenetic conservation and divergence. *Nature* **493**, 694–698 (2012).
1100 52. Nevers, Y. *et al.* Insights into ciliary genes and evolution from multi-level
1101 phylogenetic profiling. *Mol. Biol. Evol.* **34**, 2016–2034 (2017).
1102 53. McLaughlin, L. S., Haft, R. J. F. & Forest, K. T. Structural insights into the Type

1103 II secretion nanomachine. *Current Opinion in Structural Biology* **22**, 208–216
1104 (2012).
1105 54. Okuno, D., Iino, R. & Noji, H. Rotation and structure of FoF1-ATP synthase. *J.*
1106 *Biochem.* **149**, 655–664 (2011).
1107 55. Tomko, R. J. & Hochstrasser, M. Molecular architecture and assembly of the
1108 eukaryotic proteasome. *Annu. Rev. Biochem.* **82**, 415–445 (2013).
1109 56. Babbitt, S. E., Sutherland, M. C., San Francisco, B., Mendez, D. L. & Kranz, R. G.
1110 Mitochondrial cytochrome c biogenesis: no longer an enigma. *Trends Biochem.*
1111 *Sci.* **40**, 446–55 (2015).
1112 57. Hartl, F. U., Schmidt, B., Wachter, E., Weiss, H. & Neupert, W. Transport into
1113 mitochondria and intramitochondrial sorting of the Fe/S protein of ubiquinol-
1114 cytochrome c reductase. *Cell* **47**, 939–51 (1986).
1115 58. Francisco, T. *et al.* Protein transport into peroxisomes: Knowns and unknowns.
1116 *BioEssays* **39**, 1700047 (2017).
1117 59. Nguyen, B. D. & Valdivia, R. H. Virulence determinants in the obligate
1118 intracellular pathogen *Chlamydia trachomatis* revealed by forward genetic
1119 approaches. *Proc. Natl. Acad. Sci.* **109**, 1263–1268 (2012).
1120 60. Keeling, P. J. *et al.* The marine microbial eukaryote transcriptome sequencing
1121 project (MMETSP): illuminating the functional diversity of eukaryotic life in the
1122 oceans through transcriptome sequencing. *PLoS Biol.* **12**, e1001889 (2014).
1123 61. Matasci, N. *et al.* Data access for the 1,000 Plants (1KP) project. *Gigascience* **3**, 17
1124 (2014).
1125 62. Altschul, S. F. *et al.* Gapped BLAST and PSI-BLAST: a new generation of protein
1126 database search programs. *Nucleic Acids Res.* **25**, 3389–402 (1997).
1127 63. Finn, R. D., Clements, J. & Eddy, S. R. HMMER web server: interactive sequence
1128 similarity searching. *Nucleic Acids Res.* **39**, W29-37 (2011).
1129 64. Huerta-Cepas, J., Dopazo, H., Dopazo, J. & Gabaldón, T. The human phylome.
1130 *Genome Biol.* **8**, R109 (2007).
1131 65. Emanuelsson, O., Nielsen, H., Brunak, S. & von Heijne, G. Predicting subcellular
1132 localization of proteins based on their N-terminal amino acid sequence. *J. Mol.*
1133 *Biol.* **300**, 1005–16 (2000).
1134 66. Armenteros, J. J. A. *et al.* Detecting sequence signals in targeting peptides using
1135 deep learning. *Life Sci. Alliance* **2**, (2019).
1136 67. Claros, M. G. MitoProt, a Macintosh application for studying mitochondrial
1137 proteins. *Comput. Appl. Biosci.* **11**, 441–7 (1995).
1138 68. Fukasawa, Y. *et al.* MitoFates: improved prediction of mitochondrial targeting
1139 sequences and their cleavage sites. *Mol. Cell. Proteomics* **14**, 1113–26 (2015).
1140 69. Neuberger, G., Maurer-Stroh, S., Eisenhaber, B., Hartig, A. & Eisenhaber, F.
1141 Prediction of peroxisomal targeting signal 1 containing proteins from amino acid
1142 sequence. *J. Mol. Biol.* **328**, 581–92 (2003).
1143 70. Käll, L., Krogh, A. & Sonnhammer, E. L. L. Advantages of combined
1144 transmembrane topology and signal peptide prediction--the Phobius web server.
1145 *Nucleic Acids Res.* **35**, W429-32 (2007).
1146 71. Finn, R. D. *et al.* The Pfam protein families database: towards a more sustainable
1147 future. *Nucleic Acids Res.* **44**, D279-85 (2016).
1148 72. de Lima Morais, D. A. *et al.* SUPERFAMILY 1.75 including a domain-centric

1149 gene ontology method. *Nucleic Acids Res.* **39**, D427-34 (2011).
1150 73. Frickey, T. & Lupas, A. CLANS: a Java application for visualizing protein
1151 families based on pairwise similarity. *Bioinformatics* **20**, 3702–3704 (2004).
1152 74. Edgar, R. C. MUSCLE: multiple sequence alignment with high accuracy and high
1153 throughput. *Nucleic Acids Res.* **32**, 1792–7 (2004).
1154 75. Katoh, K. & Standley, D. M. MAFFT multiple sequence alignment software
1155 version 7: improvements in performance and usability. *Mol. Biol. Evol.* **30**, 772–
1156 780 (2013).
1157 76. Abby, S. S. *et al.* Identification of protein secretion systems in bacterial genomes.
1158 *Sci. Rep.* **6**, 23080 (2016).
1159 77. Criscuolo, A. & Gribaldo, S. BMGE (Block Mapping and Gathering with
1160 Entropy): a new software for selection of phylogenetic informative regions from
1161 multiple sequence alignments. *BMC Evol. Biol.* **10**, 210 (2010).
1162 78. Nguyen, L.-T., Schmidt, H. A., von Haeseler, A. & Minh, B. Q. IQ-TREE: a fast
1163 and effective stochastic algorithm for estimating maximum-likelihood
1164 phylogenies. *Mol. Biol. Evol.* **32**, 268–74 (2015).
1165 79. Lartillot, N. & Philippe, H. A Bayesian mixture model for across-site
1166 heterogeneities in the amino-acid replacement process. *Mol. Biol. Evol.* **21**, 1095–
1167 109 (2004).
1168 80. Bienert, S. *et al.* The SWISS-MODEL Repository-new features and functionality.
1169 *Nucleic Acids Res.* **45**, D313–D319 (2017).
1170 81. Guex, N., Peitsch, M. C. & Schwede, T. Automated comparative protein structure
1171 modeling with SWISS-MODEL and Swiss-PdbViewer: A historical perspective.
1172 *Electrophoresis* **30**, S162–S173 (2009).
1173 82. Biasini, M. *et al.* SWISS-MODEL: modelling protein tertiary and quaternary
1174 structure using evolutionary information. *Nucleic Acids Res.* **42**, W252-8 (2014).
1175 83. Jedelský, P. L. *et al.* The minimal proteome in the reduced mitochondrion of the
1176 parasitic protist *Giardia intestinalis*. *PLoS One* **6**, e17285 (2011).
1177 84. Černá, M., Kuntová, B., Talacko, P., Stopková, R. & Stopka, P. Differential
1178 regulation of vaginal lipocalins (OBP, MUP) during the estrous cycle of the house
1179 mouse. *Sci. Rep.* **7**, 11674 (2017).
1180 85. Cox, J. *et al.* Accurate proteome-wide label-free quantification by delayed
1181 normalization and maximal peptide ratio extraction, termed MaxLFQ. *Mol. Cell.*
1182 *Proteomics* **13**, 2513–2526 (2014).
1183 86. Tyanova, S. *et al.* The Perseus computational platform for comprehensive analysis
1184 of (prote)omics data. *Nat. Methods* **13**, 731–740 (2016).
1185 87. Dunkley, T. P. J., Watson, R., Griffin, J. L., Dupree, P. & Lilley, K. S.
1186 Localization of organelle proteins by isotope tagging (LOPIT). *Mol. Cell.*
1187 *Proteomics* **3**, 1128–1134 (2004).
1188 88. Zubáčová, Z., Krylov, V. & Tachezy, J. Fluorescence in situ hybridization (FISH)
1189 mapping of single copy genes on *Trichomonas vaginalis* chromosomes. *Mol.*
1190 *Biochem. Parasitol.* **176**, 135–137 (2011).
1191 89. Poon, S. K., Peacock, L., Gibson, W., Gull, K. & Kelly, S. A modular and
1192 optimized single marker system for generating *Trypanosoma brucei* cell lines
1193 expressing T7 RNA polymerase and the tetracycline repressor. *Open Biol.* **2**,
1194 110037 (2012).

90. Brun, R. & Schönenberger. Cultivation and *in vitro* cloning or procyclic culture forms of Trypanosoma brucei in a semi-defined medium. Short communication. *Acta Trop.* **36**, 289–92 (1979).
91. Kaurov, I. *et al.* The diverged trypanosome MICOS complex as a hub for mitochondrial cristae shaping and protein import. *Curr. Biol.* **28**, 3393-3407.e5 (2018).
92. Studier, F. W. Protein production by auto-induction in high-density shaking cultures. (2005). doi:10.1016/j.pep.2005.01.016
93. Seydlová, G. *et al.* Lipophosphonoxins II: design, synthesis, and properties of novel broad spectrum antibacterial agents. *J. Med. Chem.* **60**, 6098–6118 (2017).
94. Nicolai, C. & Sachs, F. Solving ion channel kinetics with the QuB software. *Biophys. Rev. Lett.* **08**, 191–211 (2013).
95. Pyrihová, E. *et al.* A Single Tim translocase in the mitosomes of *Giardia intestinalis* illustrates convergence of protein import machines in anaerobic eukaryotes. *Genome Biol. Evol.* **10**, 2813–2822 (2018).
96. Daum, G., Böhni, P. C. & Schatz, G. Import of proteins into mitochondria. Cytochrome b2 and cytochrome c peroxidase are located in the intermembrane space of yeast mitochondria. *J. Biol. Chem.* **257**, 13028–13033 (1982).
97. Dolezal, P. *et al.* Legionella pneumophila secretes a mitochondrial carrier protein during infection. *PLoS Pathog.* **8**, e1002459 (2012).
98. Battesti, A. & Bouveret, E. The bacterial two-hybrid system based on adenylate cyclase reconstitution in *Escherichia coli*. *Methods* **58**, 325–334 (2012).
99. Miller, J. H. *Experiments in molecular genetics*. (Cold Spring Harbor Laboratory, 1972).
100. Fields, S. & Song, O. A novel genetic system to detect protein-protein interactions. *Nature* **340**, 245–246 (1989).
101. Vizcaíno, J. A. *et al.* 2016 update of the PRIDE database and its related tools. *Nucleic Acids Res.* **44**, 11033–11033 (2016).
102. Adl, S. M. *et al.* Revisions to the classification, nomenclature, and diversity of eukaryotes. *J. Eukaryot. Microbiol.* **66**, 4–119 (2019).
103. Strassert, J. F. H., Jamy, M., Mylnikov, A. P., Tikhonenkov, D. V & Burki, F. New Phylogenomic Analysis of the Enigmatic Phylum Telonemia Further Resolves the Eukaryote Tree of Life. *Mol. Biol. Evol.* **36**, 757–765 (2019).

Acknowledgements

We would like to thank Michelle Leger and Alastair Simpson for granting us access, prior to publication, to their transcriptomic data from *A. godoyi* and *G. okellyi*, respectively, data that were instrumental in annotating the Gsp and Gcp genes in our genome assemblies. This work was supported by Czech Science Foundation grants 13-29423S to PD and 18-18699S to ME, and the KONTAKT II grant LH15253 provided by Ministry of Education, Youth and Sports of CR (MEYS) to PD. This work was also supported by MEYS within the National Sustainability Program II (Project BIOCEV-FAR, LQ1604) the project BIOCEV (CZ.1.05/1.1.00/02.0109), and the project "Centre for research of pathogenicity and virulence of parasites" (No. CZ.02.1.01/0.0/0.0/16_019/0000759) funded by European Regional Development Fund (ERDF) and MEYS and by Moore-

Simons Project on the Origin of the Eukaryotic Cell to PD. The work in the OF laboratory was funded by the ANR-14-CE09-0004 grant. JP was supported by a grant from the Gordon and Betty Moore Foundation to ADT. This work was supported by The Ministry of Education, Youth and Sports from the Large Infrastructures for Research, Experimental Development and Innovations project "IT4Innovations National Supercomputing Center – LM2015070".

Author information

Affiliations

Department of Parasitology, Faculty of Science, Charles University, BIOCEV, Průmyslová 595, Vestec, 252 42, Czech Republic
L. Horváthová, V. Žárský, A. Krupičková, V. Klápšťová, M. Vinopalová, L. Marková, L. Voleman, M. Petrů, Z. Vaitová & P. Doležal

Department of Biology and Ecology, Faculty of Science, University of Ostrava, Chittussiho 10, 710 00 Ostrava, Czech Republic
T. Pánek, V. Klimeš & M. Eliáš

School of Biosciences, University of Birmingham, Edgbaston, B15 2TT, UK
R. Derelle

Laboratory of Molecular & Evolutionary Parasitology, RAPID group, School of Biosciences, University of Kent, Canterbury, CT2 7NZ, UK
J. Pyrih & A. D. Tsaousis

Department of Zoology, Faculty of Science, Charles University, Viničná 7, Prague 2, 128 44, Czech Republic
I. Čepička

Department of Genetics and Microbiology, Faculty of Science, Charles University, Viničná 7, Prague 2, 128 44, Czech Republic
K. Hryzáková

Proteomic core facility, Faculty of Science, Charles University, BIOCEV, Průmyslová 595, Vestec, 252 42, Czech Republic
K. Harant

Department of Biochemistry and Molecular Biology and Centre for Comparative Genomics and Evolutionary Bioinformatics, Dalhousie University, Halifax, NS B3H 4R2, Canada
M. W. Gray

Center for Cellular Imaging and NanoAnalytics, University of Basel, Mattenstrasse 26, CH-4058 Basel, Switzerland
M. Chami

Institut Pasteur, Biochemistry of Macromolecular Interactions Unit, Department of Structural Biology and Chemistry, CNRS UMR3528, 75015 Paris, France
I. Guilvout & O. Francetic

Robert Cedergren Centre for Bioinformatics and Genomics, Département de Biochimie, Université de Montréal, Montreal, QC, Canada H3T 1J4
B. F. Lang

Institute of Molecular Genetics, Czech Academy of Sciences, 142 20 Prague 4, Czech Republic
Č. Vlček

Author contributions

L.H. planned and carried out the experiments, V.Ž. conceived the original idea and carried out the bioinformatics analyses, T.P. obtained the *N. damariscottae* genome sequence and carried out the genome and bioinformatic analyses, R.D. designed and carried out comparative genomic analyses, J.P. planned and carried out the experiments on *N. gruberi* mitochondrial proteome and analysed the data, A.M. carried out the experiments, Ve.K. carried out the experiments, M.V. carried out the experiments, L.M. carried out the experiments, L.V. carried out the experiments Vl.K. participated in genome sequencing and analysis, M.P. planned carried out the experiments, I.Č. participated in genome data acquisition, K.H. carried out the experiments, Z.V. carried out the experiments, K.H. analysed the proteome of *N. gruberi* mitochondria, M.W.G. contributed to the interpretation of the results and manuscript preparation, M.CH. carried out the experiments and analyzed the data, I.G. designed and planned the experiments, O.F. designed, planned and carried out the experiments and analyzed the data, B.F.L. provided the genome data and analyses and contributed to manuscript preparation, Č.V. participated in genome data acquisition, A.D.T. designed and planned the experiments, M.E. conceived the idea, performed genomic analyses and wrote the manuscript, P.D. conceived the idea, designed and performed experiments and wrote the manuscript.

Competing interests

None declared.

Corresponding author

Correspondence to M. Eliáš or P. Doležal.

Figure Legends

Fig. 1 Some eukaryotes harbour homologues of core components of the bacterial T2SS machinery. (A) Schematic representation of the complete bacterial T2SS; subunits having identified eukaryotic homologues are highlighted in colour. For simplicity, GspDN represents in the figure three different eukaryotic proteins (GspDN1 to GspDN3), together corresponding to two versions of a conserved domain present as a triplicate in the N-terminal region of the bacterial GspD protein. (B) Phylogenetic distribution of eukaryotic homologues of bacterial T2SS subunits (Gsp proteins) and co-occurring proteins (Gcp). Core T2SS components (cyan), eukaryote-specific T2SS components (dark blue), Gcp proteins carrying protein domains found in eukaryotes (magenta), and Gcp proteins without discernible homologues or with homologues only in prokaryotes (pink). Coloured sections indicate proteins found to be present in genome or transcriptome data; white sections, proteins absent from complete genome data; grey sections, proteins absent from transcriptome data. The asterisk indicates the presence of the particular protein in at least two of the three *Percolomonas* or at least one of the two Hemimastigophora species analyzed. The species name in parentheses has not yet been formally published. Sequence IDs and additional details on the eukaryotic Gsp and Gcp proteins are provided in Supplementary Table 1. The tree topology and taxon names reflect most recent phylogenomic studies of eukaryotes[32,102,103]; the root (LECA) is placed according to ref. [29].

Fig. 2 Eukaryotic Gsp homologues are monophyletic. Maximum likelihood (ML) phylogenetic tree of eukaryotic and selected bacterial GspG proteins demonstrating the monophyletic origin of the eukaryotic GspG proteins and their separation from bacterial homologues by a long branch (the tree inferred using IQ-TREE). Branch support (bootstrap) was assessed by ML ultrafast bootstrapping and is shown only for branches where support is > 50.

Fig. 3 Eukaryotic T2SS components are localized in mitochondria. (A) *S. cerevisiae* expressing *G. okellyi* and *N. gruberi* Gsp proteins as C-terminal GFP fusions stained with MitoTracker red CMX ROS to visualize mitochondria. (B) Expression of *G. okellyi* GspD and GspG2 with the C-terminal V5 Tag in *T. brucei* visualized by immunofluorescence; the cells are co-stained with MitoTracker red. (C) Cellular fractions of *N. gruberi* labelled by specific polyclonal antibodies raised against GspG1, GspEN2A and mitochondrial (alternative oxidase – AOX, TatC,) cytosolic (hemerythrin) marker proteins. (D) Immunofluorescence microscopy of *N. gruberi* labelled with specific polyclonal antibodies raised against GspG1 and GspEN2A, and co-stained with MitoTracker red. Scale bar (parts A-D), 10 µm. (E) PCA analysis of 4,198 proteins identified in the proteomic analysis of *N. gruberi* subcellular fractions differentially enriched in mitochondria. The cluster of mitochondrial proteins was defined on the basis of 376 mitochondrial markers. The boundaries of the cluster of co-purified peroxisomal proteins were defined by 26 peroxisomal markers.

Fig. 4 Mitochondrial GspD oligomerizes towards the formation of membrane pores. (A) Domain architecture of the canonical bacterial GspD and the eukaryotic proteins homologous to its different parts (short N-terminal region of mitochondrial GspD of unidentified homology shown in grey). Below, protein sequence alignment of the secretin C-domain of bacterial and mitochondrial orthologues (mitochondrial GspD or GspDL and the respective molecular complex of bacterial secretins is depicted in grey, the numbers on the right depict the position of the amino acid in the particular sequence). (B) *In vitro* import of *Ng*GspD into isolated yeast mitochondria over a period of 16 min. Dissipation of the membrane potential (ΔΨ) by AVO mix abolished the import of matrix reporter protein (Su9-DHFR) bud did not affect the mitochondrial GspD; p – precursor of Su9-DHFR, m – mature form of the protein upon cleavage of the mitochondrial targeting sequence. (C) Structural model of *Go*GspD built by ProMod3 on the *Vibrio cholerae* GspD template. Top and side view of a cartoon and a transparent surface representation of the *Go*GspD pentadecamer model is shown in blue. The amphipathic helical loop (AHL), a signature of the secretin family, is highlighted and coloured according to the secondary structure with strands in magenta, helices in cyan and loops in light brown. The C-terminal GpsD residues are highlighted as spheres. The detailed view of the AHL region shows the essential residues V162 and F166 pointing towards the membrane surface. (D) *In vitro* translation and assembly of mitochondrial *Go*GspD into a high-molecular-weight complex; lipo – liposomes added, urea – liposome fraction after 2M urea treatment. (E) Y2H assay suggests the self- and mutual interaction of *Ng*GspD and *Ng*GspDN1.

Fig. 5 Membrane pore formation of mitochondrial GspD. (A) Expression of mitochondrial *Ng*GspD in bacteria quickly causes cell death upon induction. (B) Size exclusion chromatography of *Ng*GspD shows two peaks of putative GspD complexes (bottom) and SDS-PAGE of the corresponding fractions (top). (C) Single channel recording of the *Ng*GspD complex. The applied membrane potential was 15 mV. (D) Histogram of different recorded amplitudes during channel opening indicates multiple types of *Ng*GspD-formed pores in the membrane.

Fig. 6 Structure and maturation of mitochondrial GspG. (A) Domain architecture of the bacterial and the mitochondrial pseudopilin GspG (top). The arrow indicates the processing site of the bacterial GspG during protein maturation. MTS – mitochondria targeting sequence, + – polar anchor, TMD – transmembrane domain, ND – novel domain. (Bottom) Protein sequence alignment of the pseudopilin domains of mitochondrial and bacterial GspG proteins (in case two paralogues are present, only GspG1 is shown) (B) Homology modelling of *Go*GspG1. Top: pairwise alignment of protein sequences of *Go*GspG1 and *Klebisella oxytoca* PulG (the template used in model building). Regions of high sequence similarity are highlighted, including the hydrophobic segment (cyan), the α-β loop (magenta) and GspG signature loop with conserved Pro residues (green). Bottom: side and top views of the cartoon and transparent surface representation of *Go*GspG pilus model based on the pseudopilus cryo-EM reconstruction[47]. Proteins are coloured based on the secondary structure, with helix regions in cyan and loops in light brown. The regions of GspG1 sharing high similarity with PulG are highlighted with the same colour code as in the sequence alignment, with side chains shown in magenta and green. Inset: Detail of the structurally conserved loop regions. The novel domain (ND) specific to mitochondrial GspG proteins was omitted from the modelling. (C) Peptides specific to *Ng*GspG1 retrieved from the proteomic analysis of *N. gruberi* mitochondria. The Leu residue highlighted in blue indicates residue +1 following the processing site of bacterial GspG proteins.

Fig. 7 The protein interactions of mitochondrial GspG. (A) The soluble part of the pseudopilin domain was purified to homogeneity on and ran through a gel filtration column, which demonstrated the stable monomeric state of the protein. (B) Thermophoresis of NT-647-labelled protein showed specific self-interaction of the domain (top); plotting of the change in thermophoresis yielded a K_d of 216 ± 15.1 nm, concentration of the labelled GspG was 10 nM (bottom). (C) Positive interaction between the mitochondrial GspG protein and other mitochondrial T2SS subunits as determined by the BACTH assay. The error bars depict standard error of mean.

Fig. 8 Proteins with the same phylogenetic profile as the originally identified mitochondrial Gsp homologues. (A) Schematic domain representation of 23 proteins occurring in heteroloboseans, jakobids and malawimonads with the core T2SS subunits but not in other eukaryotes analyzed. Proteins with a functional link to the T2SS suggested by sequence homology are shown in blue, proteins representing novel paralogues within broader (super)families are shown in violet, and proteins without discernible homologues or with homologues only in prokaryotes are shown in pink. The presence of conserved protein domains or characteristic structural motifs is shown if detected in the given protein. Grey block – predicted transmembrane domain (see also Supplementary Fig. 11); "C H C H" – the presence of absolutely conserved cysteine and histidine residues (see also Supplementary Fig. 12) that may mediate binding of a prosthetic group; "HEXXH" and "EXXA" in Gcp16 indicate absolutely conserved motifs suggesting that the protein is a metallopeptidase of the gluzincin group (see text). The length of the rectangles corresponds to the relative size of the proteins. (B) Protein sequence alignment of Gcp12 proteins with highlighted conserved cysteine (black circles)

and histidine (red circles) residues. (C) The expression of *Go*Gcp12 in *T. brucei* with the C-terminal V5 tag (green) showed partial co-localization with the mitochondrion (red).

Fig. 9 The mitochondrial T2SS (miT2SS) as part of a hypothetical eukaryotic functional pathway connecting the mitochondrion and the peroxisome. The scheme presents the most reasonable interpretation of the findings reported in this study, but further work is needed to test details of the working model. According to the model, a nucleus-encoded protein (green), possibly one of the newly identified Gcp proteins, is imported via the TOM complex into the mitochondrial inner membrane space, where it is modified by addition of a specific prosthetic group. After folding it becomes a substrate of the miT2SS machinery, is exported from the mitochondrion and finally reaches the peroxisome. The loading of the prosthetic group, the delivery to the peroxisome and possibly also the actual function of the protein in the peroxisome is assisted by specific subsets of other Gcp proteins. The hypothetical presence of Gcp proteins in specific (sub)compartments is depicted as a group of orange ovals. OMM – outer mitochondrial membrane, IMS – intermembrane space, IMM – inner mitochondrial membrane, MM – mitochondrial matrix

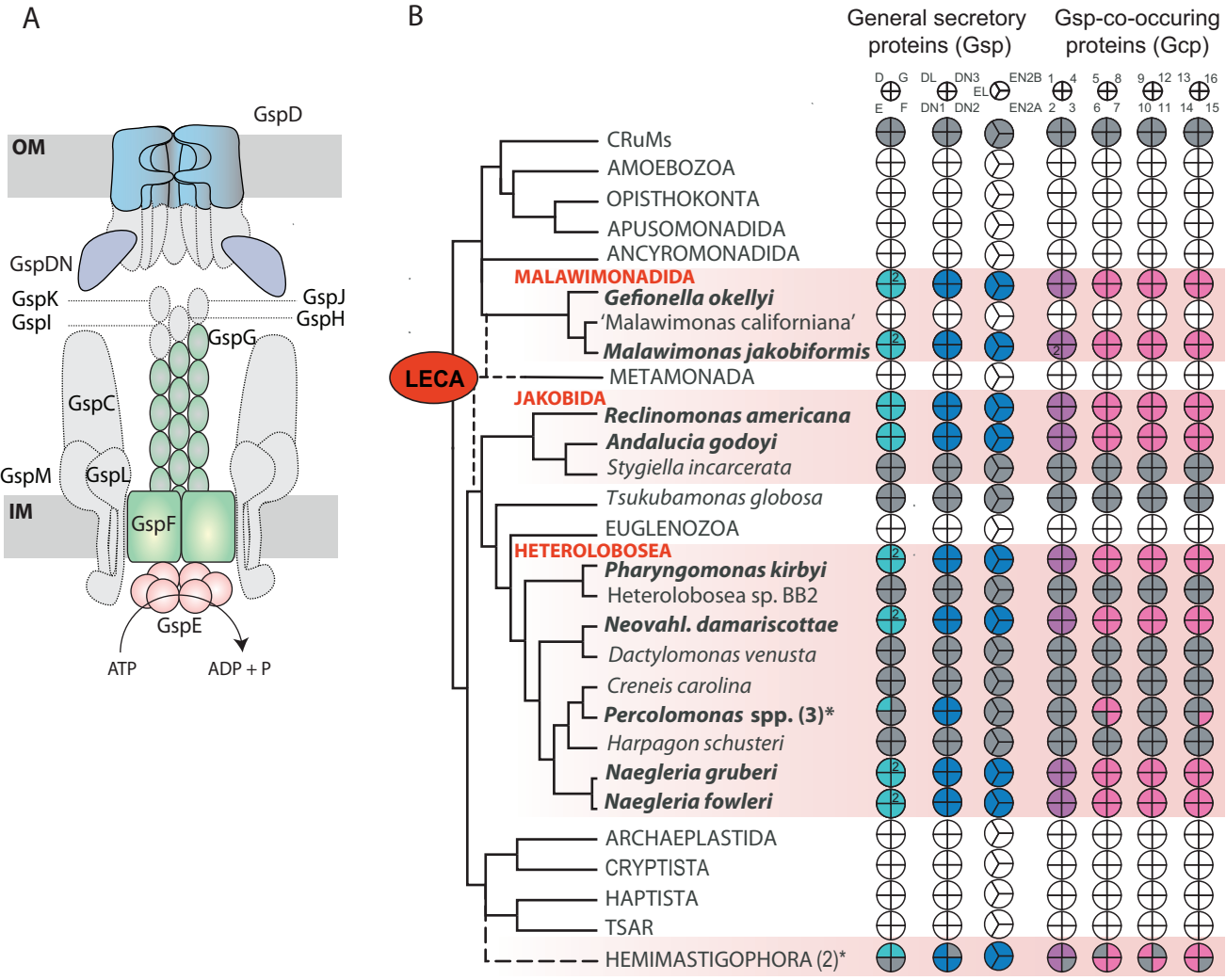
A
GspD
OM
GspDN
GspK
GspI
GspJ
GspH
GspG
GspC
GspM
GspL
IM
GspF
GspE
ATP
ADP + P
B
General secretory proteins (Gsp)
Gsp-co-occuring proteins (Gcp)
D G
E F
DL DN3
DN1 DN2
EL
EN2B
EN2A
1 4
2 3
5 8
6 7
9 12
10 11
13 16
14 15
CRuMs
AMOEBOZOA
OPISTHOKONTA
APUSOMONADIDA
ANCYROMONADIDA
MALAWIMONADIDA
Gefionella okellyi
'Malawimonas californiana'
Malawimonas jakobiformis
LECA
METAMONADA
JAKOBIDA
Reclinomonas americana
Andalucia godoyi
Stygiella incarcerata
Tsukubamonas globosa
EUGLENOZOA
HETEROLOBOSEA
Pharyngomonas kirbyi
Heterolobosea sp. BB2
Neovahl. damariscottae
Dactylomonas venusta
Creneis carolina
Percolomonas spp. (3)*
Harpagon schusteri
Naegleria gruberi
Naegleria fowleri
ARCHAEPLASTIDA
CRYPTISTA
HAPTISTA
TSAR
HEMIMASTIGOPHORA (2)*

Figure 1

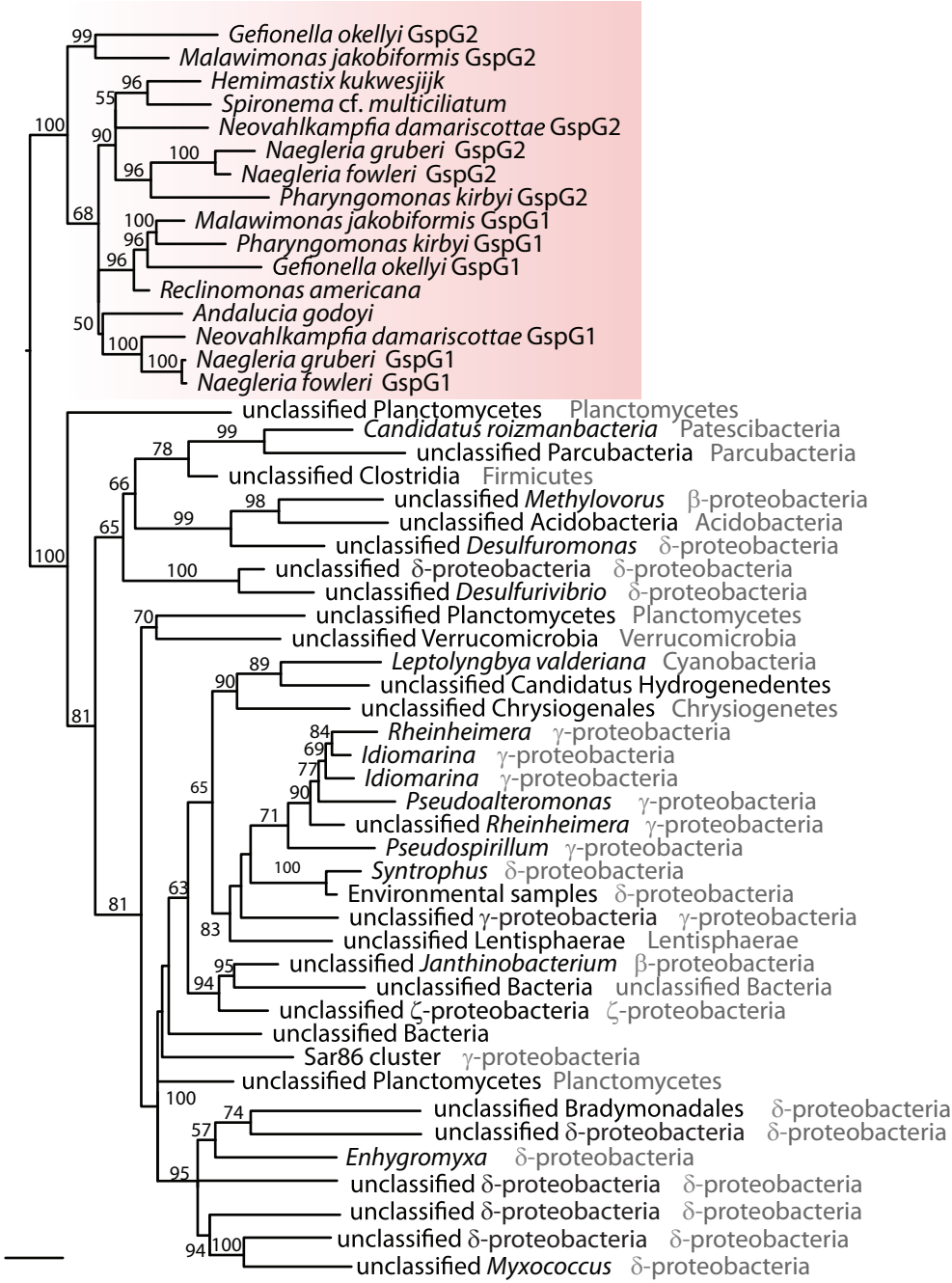
Gefionella okellyi GspG2
Malawimonas jakobiformis GspG2
Hemimastix kukwesjijk
Spironema cf. multiciliatum
Neovahlkampfia damariscottae GspG2
Naegleria gruberi GspG2
Naegleria fowleri GspG2
Pharyngomonas kirbyi GspG2
Malawimonas jakobiformis GspG1
Pharyngomonas kirbyi GspG1
Gefionella okellyi GspG1
Reclinomonas americana
Andalucia godoyi
Neovahlkampfia damariscottae GspG1
Naegleria gruberi GspG1
Naegleria fowleri GspG1
unclassified Planctomycetes Planctomycetes
Candidatus roizmanbacteria Patescibacteria
unclassified Parcubacteria Parcubacteria
unclassified Clostridia Firmicutes
unclassified Methylovorus β-proteobacteria
unclassified Acidobacteria Acidobacteria
unclassified Desulfuromonas δ-proteobacteria
unclassified δ-proteobacteria δ-proteobacteria
unclassified Desulfurivibrio δ-proteobacteria
unclassified Planctomycetes Planctomycetes
unclassified Verrucomicrobia Verrucomicrobia
Leptolyngbya valderiana Cyanobacteria
unclassified Candidatus Hydrogenedentes
unclassified Chrysiogenales Chrysiogenetes
Rheinheimera γ-proteobacteria
Idiomarina γ-proteobacteria
Idiomarina γ-proteobacteria
Pseudoalteromonas γ-proteobacteria
unclassified Rheinheimera γ-proteobacteria
Pseudospirillum γ-proteobacteria
Syntrophus δ-proteobacteria
Environmental samples δ-proteobacteria
unclassified γ-proteobacteria γ-proteobacteria
unclassified Lentisphaerae Lentisphaerae
unclassified Janthinobacterium β-proteobacteria
unclassified Bacteria unclassified Bacteria
unclassified ζ-proteobacteria ζ-proteobacteria
unclassified Bacteria
Sar86 cluster γ-proteobacteria
unclassified Planctomycetes Planctomycetes
unclassified Bradymonadales δ-proteobacteria
unclassified δ-proteobacteria δ-proteobacteria
Enhygromyxa δ-proteobacteria
unclassified δ-proteobacteria δ-proteobacteria
unclassified δ-proteobacteria δ-proteobacteria
unclassified δ-proteobacteria δ-proteobacteria
unclassified Myxococcus δ-proteobacteria

Figure 2

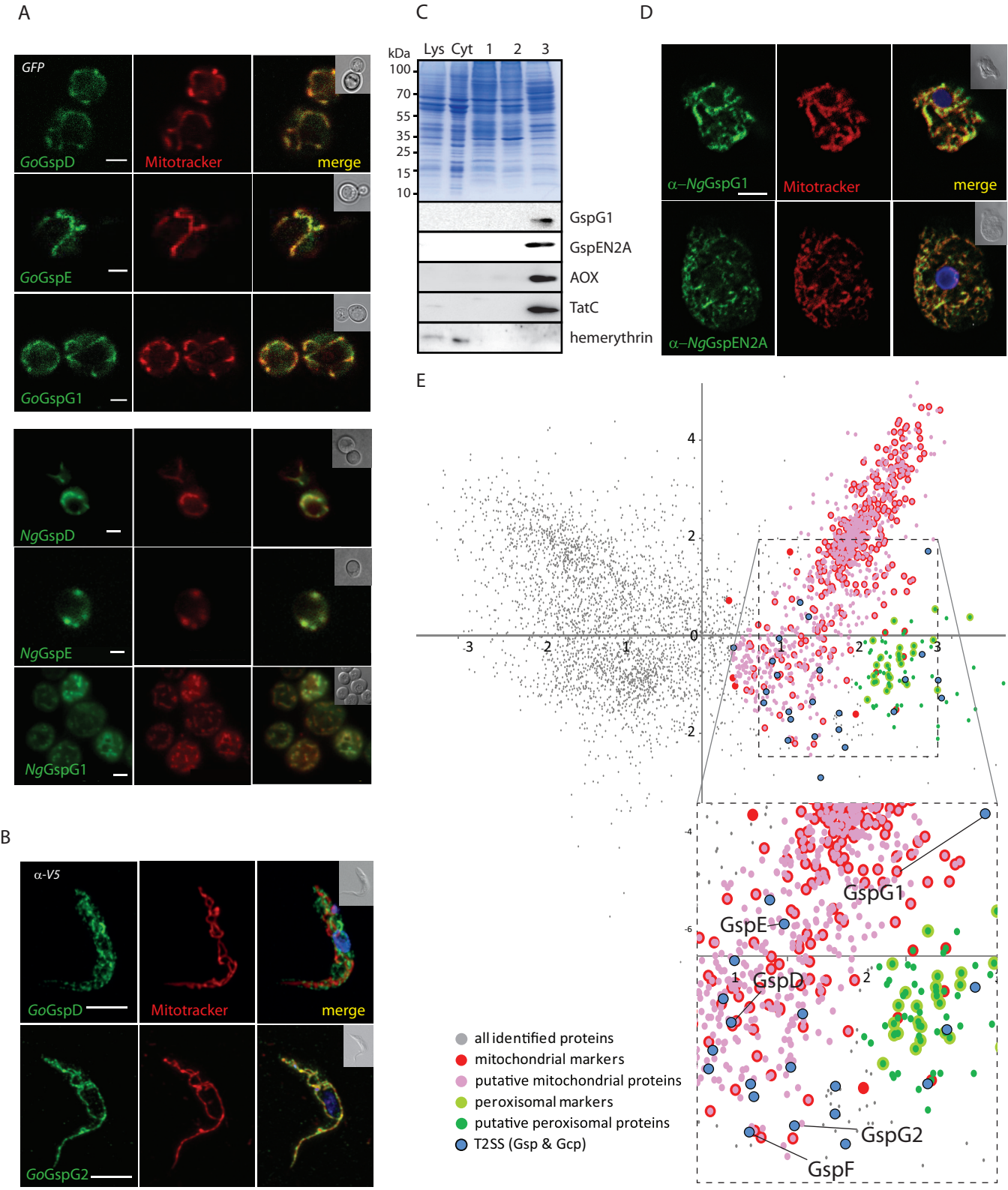
A
GFP
GoGspD
Mitotracker
merge
GoGspE
GoGspG1
NgGspD
NgGspE
NgGspG1
B
α-V5
GoGspD
Mitotracker
merge
GoGspG2
C
kDa
Lys Cyt 1 2 3
100
70
55
35
25
15
10
GspG1
GspEN2A
AOX
TatC
hemerythrin
D
α–NgGspG1
Mitotracker
merge
α–NgGspEN2A
E
all identified proteins
mitochondrial markers
putative mitochondrial proteins
peroxisomal markers
putative peroxisomal proteins
T2SS (Gsp & Gcp)
GspG1
GspE
GspD
GspG2
GspF

Figure 3

A

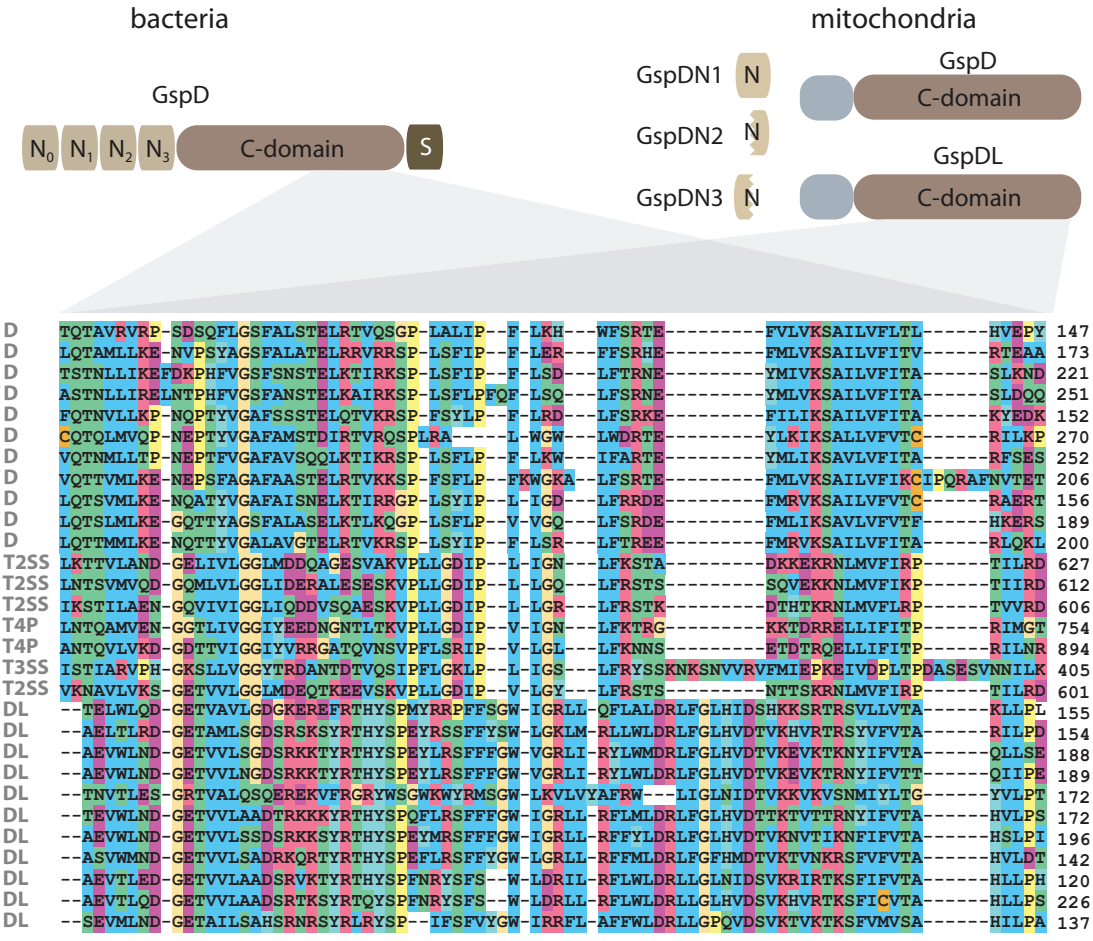

B

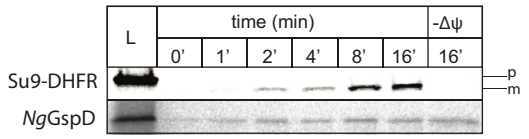

C

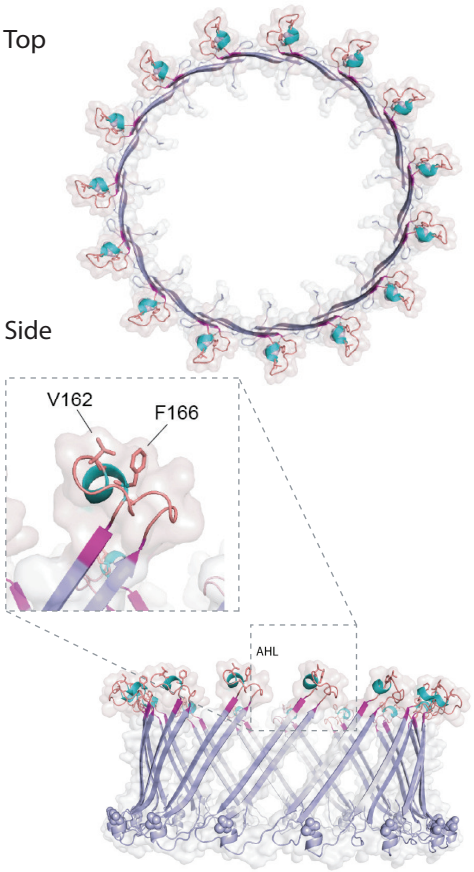

D

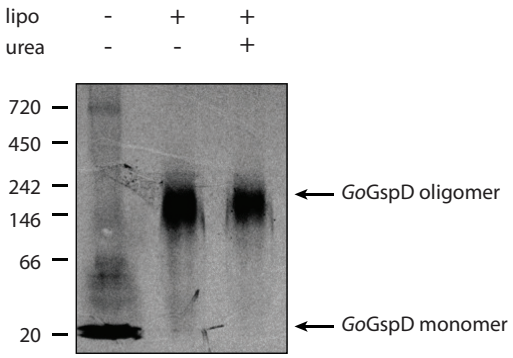

E

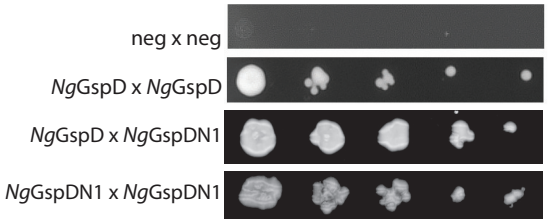

Figure 4

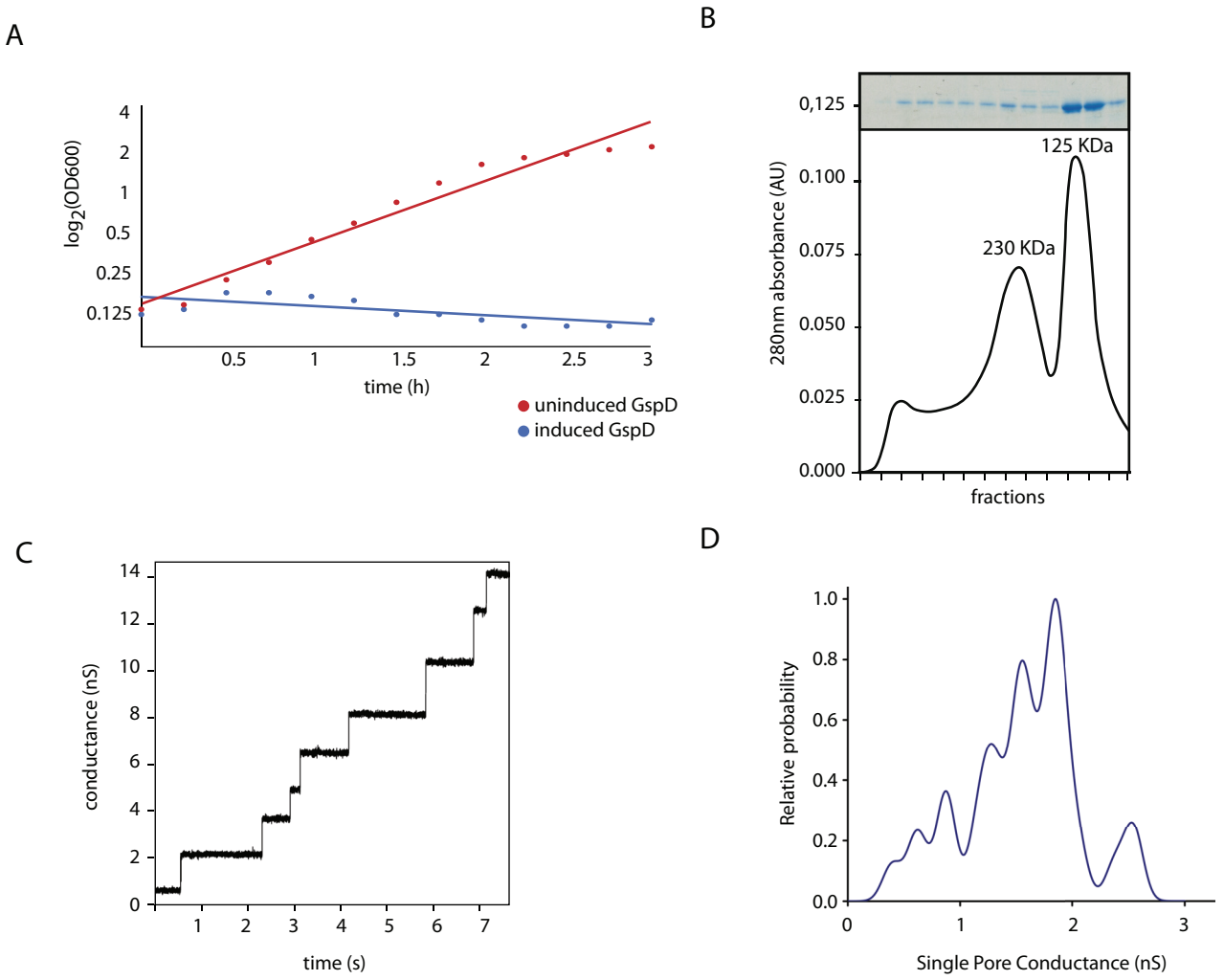
A
log2(OD600)
4
2
1
0.5
0.25
0.125
0.5
1
1.5
2
2.5
3
time (h)
uninduced GspD
induced GspD
B
0,125
0.100
0.075
0.050
0.025
0.000
280nm absorbance (AU)
125 KDa
230 KDa
fractions
C
conductance (nS)
14
12
10
8
6
4
2
0
1
2
3
4
5
6
7
time (s)
D
Relative probability
1.0
0.8
0.6
0.4
0.2
0.0
0
1
2
3
Single Pore Conductance (nS)

Figure 5

A

bacteria
mitochondria
+TMD
pseudopilin
MTS
+TMD
pseudopilin
ND
+
*
TMD
A. godoyi
R. americana
M. jakobiformis GspG1
G. okellyi GspG1
P. kyrbyi GspG1
N. gruberi GspG1
N. fowleri GspG1
N. damariscottae
H. kukwesjijk
S. cf. multiciliatum
E. coli
K. pneumoniae
V. cholerae
L. pneumophila
Caulobacter sp.

B

Target
5wda.1.A

C

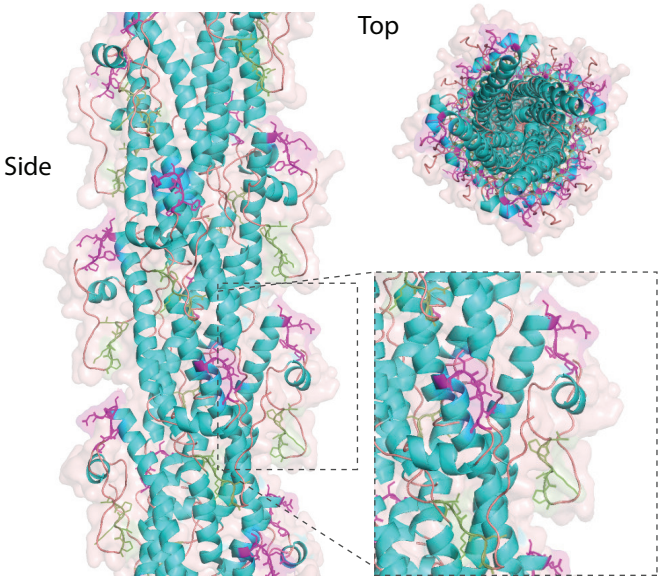
Top
Side

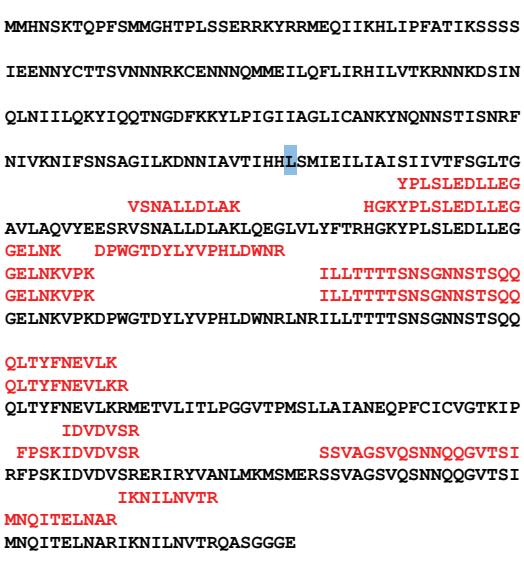

Figure 6

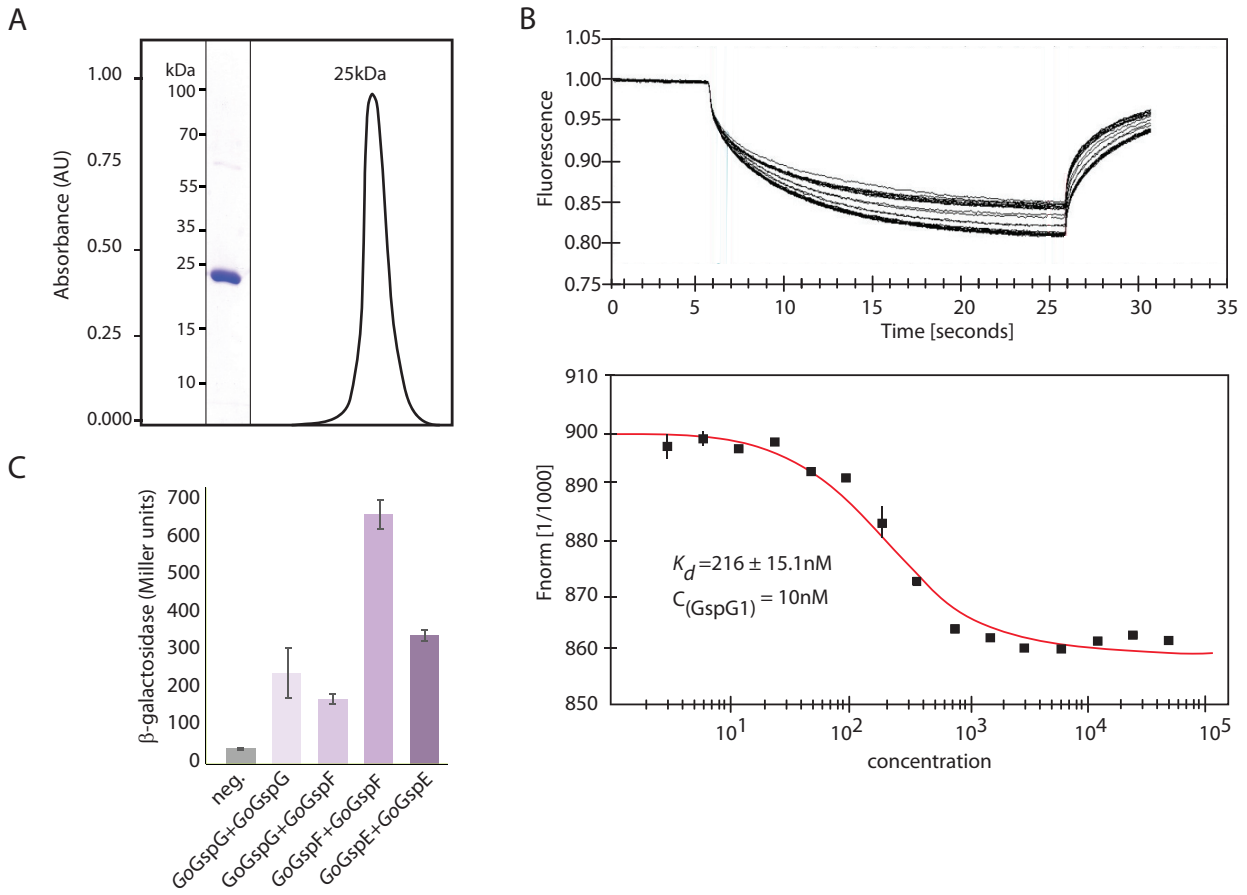
A
kDa
100
70
55
35
25
15
10
25kDa
Absorbance (AU)
1.00
0.75
0.50
0.25
0.000
B
Fluorescence
1.05
1.00
0.95
0.90
0.85
0.80
0.75
0
5
10
15
20
25
30
35
Time [seconds]
Fnorm [1/1000]
910
900
890
880
870
860
850
K_d=216 ± 15.1nM
$C_{(GspG1)}$ = 10nM
10^1
10^2
10^3
10^4
10^5
concentration
C
β-galactosidase (Miller units)
700
600
500
400
300
200
100
0
neg.
GoGspG+GoGspG
GoGspG+GoGspF
GoGspF+GoGspF
GoGspE+GoGspE

Figure 7

A

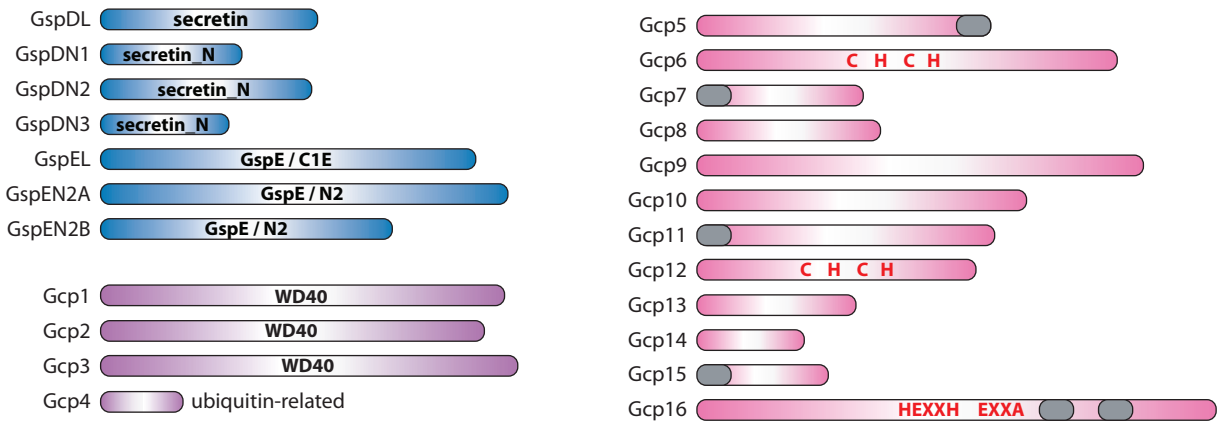
GspDL
secretin
GspDN1
secretin_N
GspDN2
secretin_N
GspDN3
secretin_N
GspEL
GspE / C1E
GspEN2A
GspE / N2
GspEN2B
GspE / N2
Gcp1
WD40
Gcp2
WD40
Gcp3
WD40
Gcp4
ubiquitin-related
Gcp5
Gcp6
C H C H
Gcp7
Gcp8
Gcp9
Gcp10
Gcp11
Gcp12
C H C H
Gcp13
Gcp14
Gcp15
Gcp16
HEXXH EXXA

B

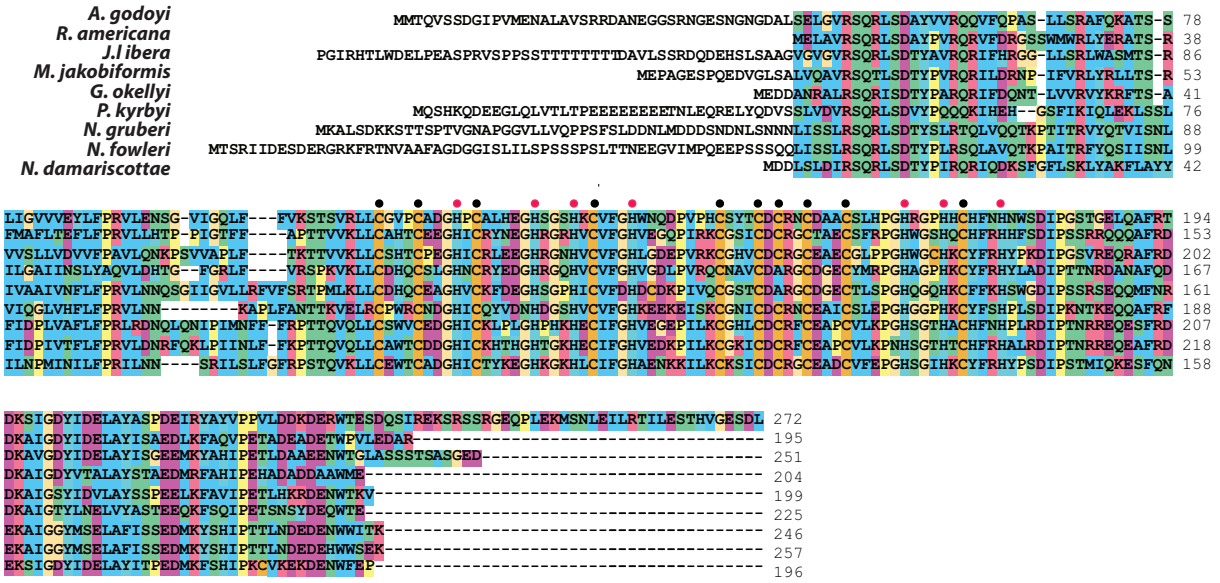
A. godoyi
R. americana
J.l ibera
M. jakobiformis
G. okellyi
P. kyrbyi
N. gruberi
N. fowleri
N. damariscottae

C

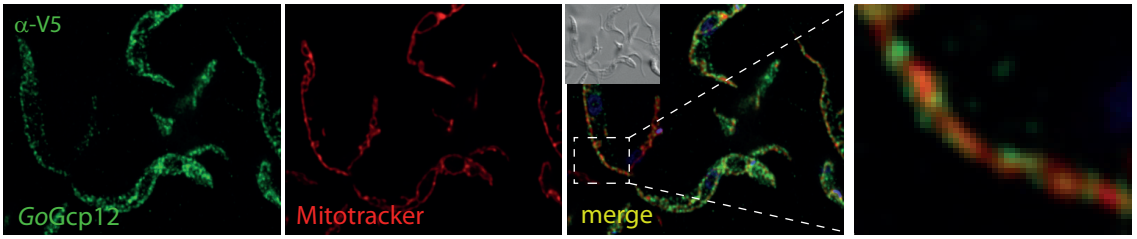
α-V5
GoGcp12
Mitotracker
merge

Figure 8

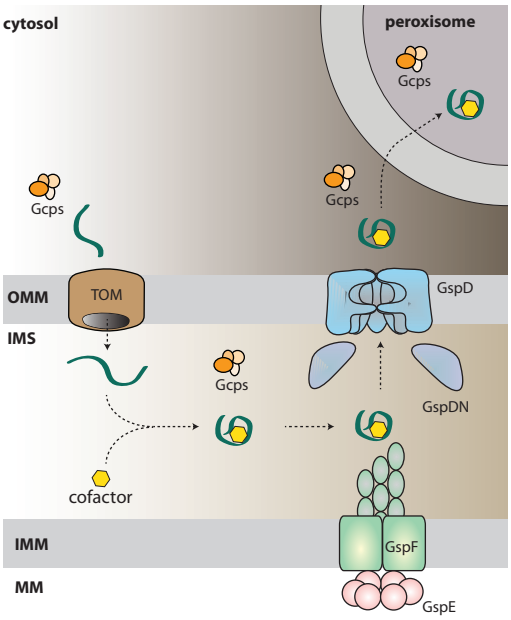
cytosol
peroxisome
Gcps
Gcps
Gcps
OMM
TOM
GspD
IMS
Gcps
GspDN
cofactor
IMM
GspF
MM
GspE

Figure 9